Thermal evolution of simple amino acids (glycine and alanine) on non-crystalline and polycrystalline ice studied by Reflection-Absorption Infrared Spectroscopy

by

Farheen Shenaz Kinoo

A thesis
presented to the University of Waterloo
in fulfillment of the
thesis requirement for the degree of
Master of Science
in
Chemistry

Waterloo, Ontario, Canada, 2009

I hereby declare that I am the sole author of this thesis. This is a true copy of the thesis, including any required final revisions, as accepted by my examiners.

Signature

I understand that my thesis may be made electronically available to the public.

Signature

Abstract

The behaviour of glycine and alanine, deposited under ultrahigh vacuum conditions onto non-crystalline ice (NCI) and polycrystalline ice (PCI) has been studied using Reflection-Absorption Infrared Spectroscopy (RAIRS). The adsorption of these molecules onto a clean polycrystalline Cu surface at 123 and 298 K has also been investigated. Both amino acids remain intact upon landing on the NCI and PCI surfaces and are present the neutral or form on these ice surfaces. Bonding to the surface occurs through the carboxylic group and the amino group initially, with the C=O and NH_2 groups involved in hydrogen bonding to the dangling OH bond of the ice surface. Multilayers are formed at higher exposure, resulting in intermolecular hydrogen bonding between the amino acid species. Upon annealing these fully covered surfaces to 150 K, the proton transfer process begins, as evidenced by the disappearance of the C=O stretching vibration band at ~1712 cm^{-1}. This phenomenon continues until the ice film is completely removed from the surface. Consequently the amino acid binds to the metal surface as a zwitterionic species. The adsorbed species then leave the surface as the substrate is annealed to higher temperature. In addition, it was shown that amino acid molecules adsorbed on the NCI do not restrict crystallization of the ice film, as supported by the appearance of the characteristic PCI ν(OH) band at 3292 cm^{-1} during annealing.

Acknowledgements

I wish to express my sincere thanks to my supervisor, Prof. K. T. Leung, for his unconditional support, guidance and help during the elaboration of this work. I am fully indebted to him for providing me all the necessary information and advice. I would also like to thank the members of my Master's Advisory committee, Professors M. Nooijen and P. Rowntree for their advice. Many thanks to Dr. M. M. Thiam for his kind help, guidance and getting me started with the machine. I would also like to express my gratitude to my parents and my brother for their ever-lasting support and encouragement. Finally I am thankful to the WATLab members for their help and support throughout the year.

Table of Contents

List of Figures

List of Tables

Chapter 1

Introduction

Adsorption of biomolecules on surfaces has been of particular interest in the past three decades in the field of surface science [1]. Surface chemistry is the discipline dealing with reactions occurring at surfaces. In the field of surface science, the base material on which processing is carried out to produce new layers of materials are usually referred to as substrates, while the molecules deposited on the surface are known as adsorbates. A typical substrate might be a metal. Adsorbates can be of various types, ranging from a simple molecule like NH_3 to a more complex one such as DNA. Since we are dealing with biomolecules as the adsorbate, the broad term "biological surface science" can thus be introduced. This term refers to the study of the properties and processes that take place between synthetic materials and biological environments and ultimately resulting in the fabrication of biofunctional surfaces [2]. A few examples of application of biological surface science are medical implants in the human body, biochips and biosensors for diagnosis, tissue engineering and bioelectronics. Figure 1.1 illustrates the set of events occurring after implantation of a medical device in the human body or a biological environment. Evidently, the first molecules to reach the surface are the water molecules, and they are followed by adsorption of proteins. When the cells arrive at the surface, they "see" a protein-covered surface. The properties of this protein layer have already been determined by the water shells formed at the surface. Therefore, cell-surface interaction refers to the interaction between the cells and surface-bound proteins or other biomolecules.

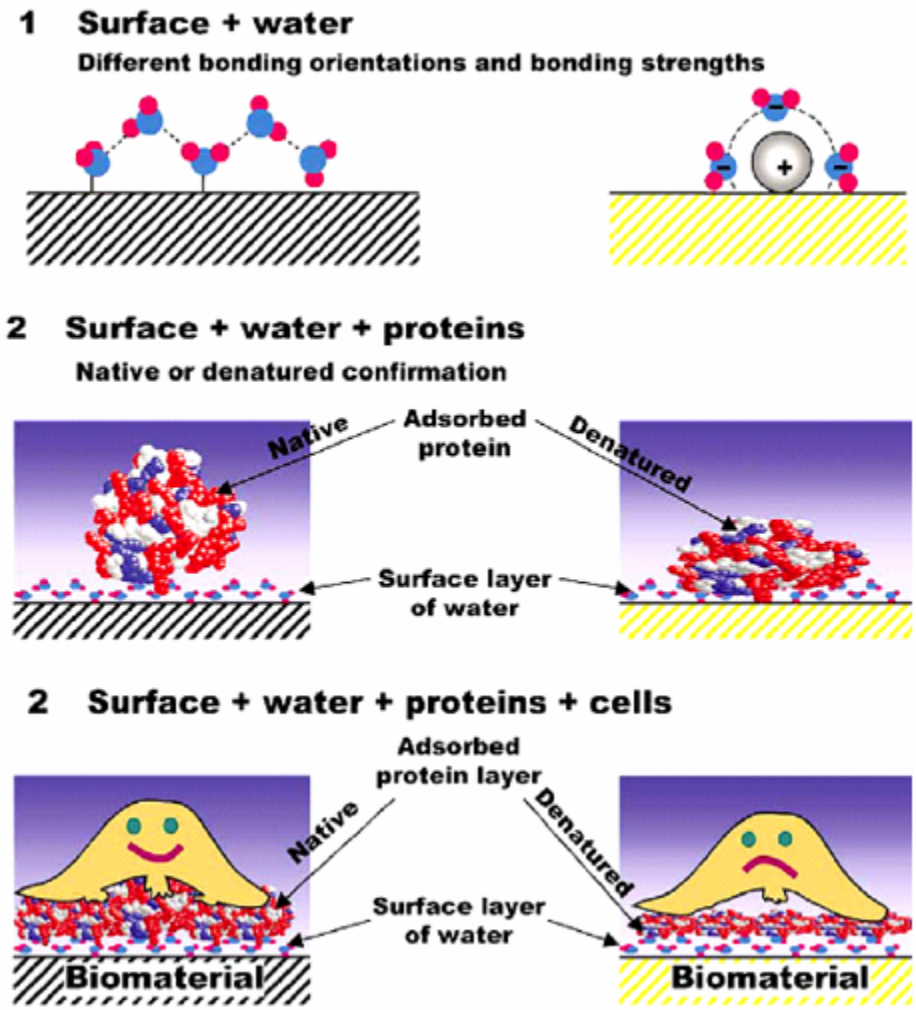

Figure 1.1: Sequence of events occurring after implantation of a medical implant in the body [2].

In the present work, we will attempt to model a similar system in which our substrate will be ice with our adsorbates being amino acid molecules. Ice has been chosen as the substrate because in addition to the IR bands existing for water, ice has an additional feature at 3696 cm^{-1}, which is related to the dangling OH bond.

This field of study is also related to the atmospheric medium or more precisely icy interstellar medium (ISM). Recently, the properties of ice have attracted much attention

with respect to the chemical processes occurring in the interstellar space. Many organic compounds have been observed in the interstellar medium [38]. Because these molecules have been detected, scientists now want to know if molecules such as amino acids or the more complex DNA exist in the interstellar medium. In fact this has been a controversial issue since Kuan et al. published an article in the Astrophysical Journal in 2004 claiming that glycine has been found in the interstellar medium [3]. However, recent studies carried out by Snyder et al. two years later, while trying to reproduce the data provided by the previous group in 2004, concluded that the previously reported information was wrong [4]. Amino acids are of particular interest because they are the building blocks of proteins, essential constituents of all organisms.

The approach adopted in our group has been to prepare well-defined ice nanolayers as the substrate, followed by the deposition of amino acid molecules and spectroscopic investigation of the as-deposited system as a function of annealing temperature. Along with earlier studies [5], ours offers complementary information about the interaction between amino acids and ice. Glycine (NH_2CH_2COOH) was used as the starting adsorbate, with ice as the substrate. Glycine is of particular interest, because it is not only a bifunctional molecule, but also the smallest amino acid. Ice has been chosen as the substrate here because it is a special surface where hydrogen bonding is known to play a key role in controlling much of ice surface chemistry. Ice can exist in two main forms, namely non-crystalline and polycrystalline ice. A polycrystalline copper disk has been used as the support to grow the ice film. Organic molecules have been embedded in or on these ice nanofilms and the thermal evolution on the ice surface can be studied by using Reflection-Absorption Infrared Spectroscopy (RAIRS). Much of the present work

has been made possible via the innovation of a high-flux neutral amino acid beam doser discussed in the experimental section. To extend the present studies on glycine, the next logical step is to study alanine particularly given that alanine is the smallest amino acid that exhibits chirality. It would therefore be of special interest to investigate whether alanine, both the L- and D- forms, will behave in a similar fashion as glycine on ice.

1.1 Structure of ice

Ice is one of the most common molecular solids existing in nature, and yet despite several studies done over the past century, much of its properties remain not fully understood [6]. The ability to establish four hydrogen bonds makes ice an exceptionally interesting system to study. In an ice structure, the H_2O molecules are arranged in a highly ordered manner such that the two H atoms of each H_2O molecule form two H-bonds with neighbouring H_2O molecules, while the two lone-pairs on the oxygen atom forms two H-bonds with two other H_2O molecules. Consequently, this results in a tetrahedral arrangement of the water molecules [7]. Ice is known to exist in at least 15 different phases [8] depending on the pressures and temperatures at which the ice is grown. Different phases of water are illustrated in the phase diagram shown in Figure 1.1. Low pressure forms of ice include non-crystalline ice, cubic ice and hexagonal ice. Increasing interest in the chemistry and physics of ice particles is due to its major role in atmospheric chemistry in addition to its environmental, interstellar and biological importance. Several methods including optical interference techniques, temperature programmed desorption, Raman spectroscopy, electron diffraction, X-ray diffraction,

neutron diffraction, infrared spectroscopy have been employed to study the structure and dynamics of ice films [9].

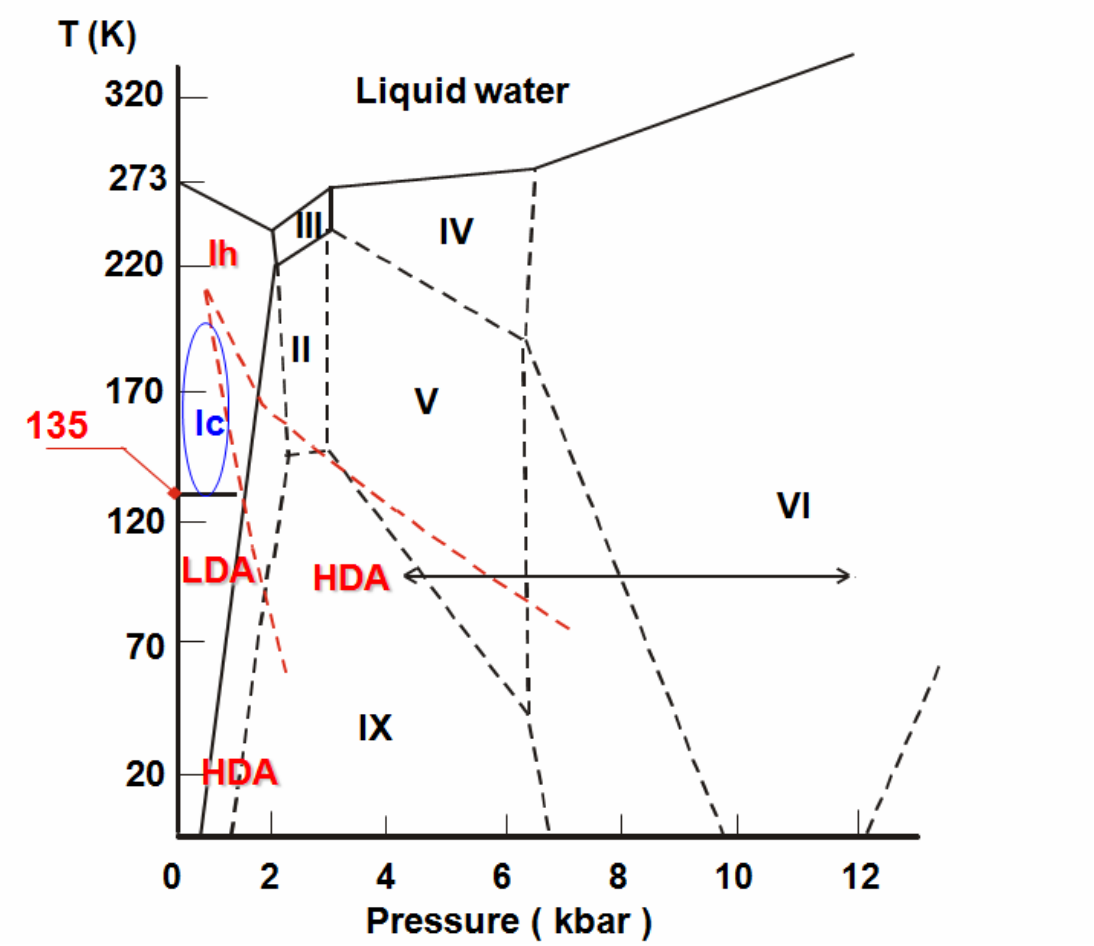

Figure 1.2: Schematic phase diagram of water.

Ice nanocrystals are said to consist of a crystalline core surrounded by surface and subsurface regions [7, 18]. It has been found that the first layer of H_2O molecules is disordered on the surface, and the transition between the surface and the organised bulk occurs through the subsurface layer, which consists of more ordered H_2O molecules establishing bent H-bonds. The subsurface layer extends towards ~3 nm from the surface [7]. It requires a minimum of 300 H_2O molecules for the crystalline structure to appear

[7]. For nanocrystals of ~20 nm diameter, ~10% of the molecules make up the surface, ~20% are in the 2–3 bilayers of the subsurface, and the rest form the bulk [18]. Figure 1.3 shows the arrangement of atoms in a crystalline ice structure.

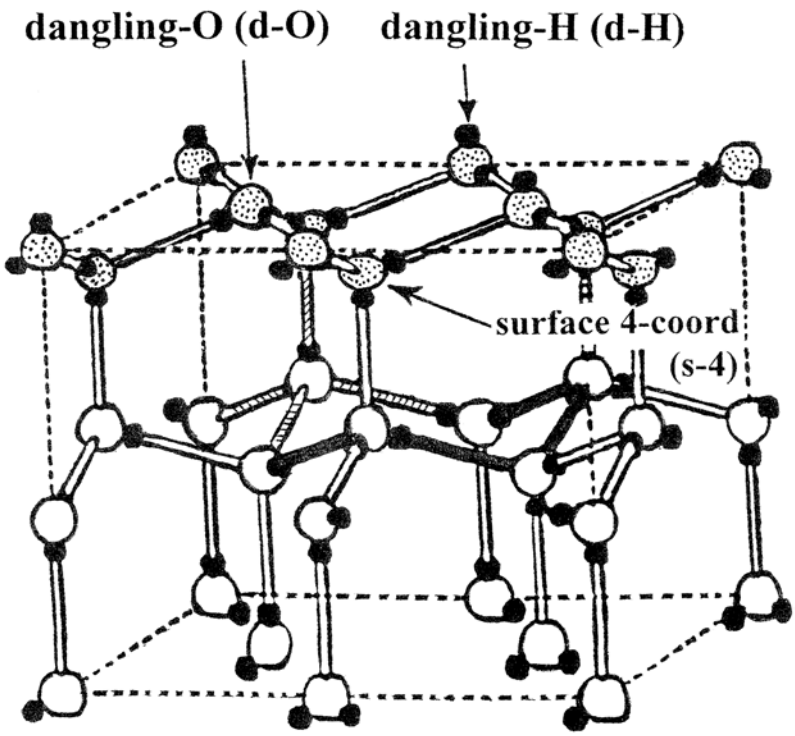

Figure 1.3: A segment of ice structure with an interior bilayer (open circles for oxygen and solid circles for hydrogen) [10].

Depositing water vapour on cold substrate at low temperature (T<130 K) and low pressure produces amorphous ice (also known as non-crystalline ice) (Figure 1.2). Interestingly, amorphous ice can be subdivided into two or possibly three different phases, depending on their density and structure. These are low-density amorphous (LDA), high-density amorphous (HDA) and very high-density amorphous (VHDA) ice, with densities of 0.94 ± 0.02 g/cm^3, 1.17 ± 0.02 g/cm^3 and 1.25 ± 0.01 g/cm^3,

respectively, at T = 77 K and P = 1 bar. [8]. At a more elevated temperature (T>130 K), polycrystalline ice can be formed [11]. Polycrystalline ice can also exist in two different polymorphs, namely cubic ice denoted as I_c and hexagonal ice, I_h, and they appear at 140–160 K and 160–240 K, respectively (Figure 1.2) [12]. An irreversible process occurs upon warming non-crystalline ice, converting it to its crystalline form over a temperature range of 140-160 K [11]. The morphology of the latter differs from the former form of ice in terms of the nanopores present within the ice structure [13]. The low-density amorphous ice is referred to as a highly porous open network with nano-scale pores and it therefore contains a significant amount of free OH groups at the surface present as the dangling OH groups, which therefore can accommodate a higher number of foreign molecules. Ice deposited at very low temperature, below 130 K, has a larger surface area and many defects, and these nanoscale micropores collapse at a higher temperature [14]. Polycrystalline ice can therefore be described as a pore-free structure because it contains essentially no pores. However, with our experimental set-up in the present work, we are able to prepare only stable cubic form of ice because as the temperature is raised, desorption of the ice film occurs before the cubic ice could be transformed to the hexagonal ice. An ice film is therefore capable of accommodating foreign molecules depending upon the structural defects existing within the ice structure.

1.2 IR spectrum of ice films

Although the structure of ice structure has been investigated by various techniques to date, infrared spectroscopy remains to be one of the most important tool in the study of the ice surface structure. There has been a large and significant amount of published vibrational spectroscopic data for ice film since the beginning of the 20th century [12,15]. X-ray diffraction studies revealed that the structure of ice consists of a very dense H-bond network [7,16]. As a first approach to understand the IR spectrum of ice, it would be useful to discuss the IR features existing for liquid water. The mid-IR spectrum of liquid water consists of three peaks associated with different types of vibration of H_2O molecules, namely, the OH stretching band [ν_s(O–H)] which is the most intense band found near 3400 cm^{-1}, the H–O–H bending mode [δ(H–O–H)] at 1640 cm^{-1} and the "libration" band [$\rho(H_2O)$] around 700 cm^{-1} [7]. The IR spectrum of ice exhibits additional peaks that are rather weak but discernible at ~3700 cm^{-1}, which is assigned to the dangling OH bonds at the interface [6], and at ~2200 cm^{-1}, referred to as the combination band. The dangling bonds are seen in both the non-crystalline and polycrystalline ice films, with a larger population observed for the former. In comparison to a non-crystalline ice film, the respective IR bands for a polycrystalline ice film usually occur at lower wavenumbers. This is mainly due to the molecular rearrangement among the H_2O molecules, which results in a strengthening of the hydrogen-bonding network in the ice structure as a non-crystalline ice film is transformed to a polycrystalline ice film [17]. In light of the differences and similarities existing between these two forms of ice films, it would be interesting to discuss the influence of certain adsorbates on these ice surfaces. This is elaborated upon in the following section.

1.3 Adsorption of molecules on ice surface

The way in which different molecules bind to the surface of ice remains of particular interest in several areas of science [18]. Gas adsorption on icy surfaces is especially important in terrestrial and atmospheric chemistry [19], while adsorbate-ice interactions are of particular interest in interstellar space sciences [18]. Although several studies have been done over the past few years in the context of ice-adsorbate systems, the study of the interaction between low-temperature water and the adsorbates at the molecular level is a relatively new topic [19,20]. Earlier work involved the study of small molecules adsorbed on an ice surface. Methane has been used as a probe molecule to observe the changes occurring upon its adsorption on porous amorphous ice at 25 K under ultra-high vacuum [14]. Ice films covered with methane involves interaction of the molecule with the surface, which was evidenced by the appearance of peaks assigned to the CH stretching vibration of methane in conjunction with the decrease in intensity of the OD stretching vibration for the ice film [14]. Saturation occurs at 1 monolayer (ML) of methane deposited on the ice at 135 K, while this is not the case for ice deposited at 25 K, which suggests different structural arrangement of particles in the ice surface at different temperatures. The modification in the infrared active bands during the adsorption of methane in addition to other small molecules on amorphous ice was also studied a few years ago. Martin et al. compared the adsorption isotherms as well as the infrared data for a number of different molecules including CH_4, N_2, CO, Ar, Kr and CF_4 adsorbed on amorphous ice [21]. N_2 and CO were thought to be involved in a stronger interaction with the ice surface compared to Ar, CH_4 and Kr, which resulted in a weakly bonded monolayer and multilayer respectively. Alterations in the observed dangling OH bond

position and intensity lead to the conclusion that these molecules are interacting with the ice surface in the following decreasing strength: CO>N_2>CH_4>Kr>Ar>CF_4, with the first three molecules showing more significant changes. Because of the strong interaction of CO with an ice surface as reported in the earlier work [21], more detailed investigation has been carried by the same group [22]. In particular, the authors compared the adsorption of CO on a bare ice surface and an ice surface covered with a pre-adsorbate, first with CF_4 and later CH_4. Basically, CO binds to the ice surface in a similar fashion, by interacting with the dangling bond in all three cases. This suggests that attraction between CO and the dangling H bond is greater than that between the dangling H (Figure 1.3) and the pre-adsorbates. In contrast, the pre-adsorbates were found to affect the way CO adsorbed on the dangling O sites. CO adsorbs less on dangling O sites for CF_4 pre-adsorption than for sole CO adsorption, and this effect is more pronounced for CH_4. In addition, Cyriac and Pradeep's work focused on the diffusive mixing of chloromethanes in different molecular solids including H_2O, D_2O and CH_3OH [23]. They concluded that due to the critical size and the hydrogen bond network of the amorphous solid water film, CCl_4 could not diffuse through the ice film. Similar observations were made for the D_2O and CH_3OH solid films. In comparison to CCl_4, the diffusivity of CH_3Cl, CH_2Cl_2 and $CHCl_3$ through these molecular solids was possible. The interaction between these chloromethanes and ice was explained in terms of the atomic charge of chlorine and molecular polarizability whereby replacement of a Cl atom by a H atom could increase on this diffusivity property.

It has been shown from previous studies [21] that small adsorbates such as N_2 and CO do not significantly influence the subsurface structure of ice. Thus it is interesting to

understand how other types of molecules interact with an ice film. In another study, the effect of H_2S and acetylene adsorbates on ice surface was investigated [24]. These molecules are known as bifunctional hydrogen bonding molecules because they can be useful as both a proton donor and a proton acceptor. Delzeit et al. observed that these adsorbates were capable of inducing ordering in the ice subsurface, by reducing the freedom of motion of the water molecules. Further studies were conducted by Devlin at al., who investigated the adsorption of three strongly H-bonding molecules, HCl, NH_3 and ethylene oxide on the surface of crystalline ice [18]. Temperature in the 20 to 125 K range was used for the adsorption of HCl on the annealed ice nanocrystals. The exposure of NH_3 and ethylene oxide to the ice surface was carried out at temperatures ranging from 120 to 130 K since both molecules are less volatile than HCl. They have shown that both NH_3 and ethylene oxide, which are referred to as small polar guest molecules, adsorbed as molecular complexes with the ice surface sites, ultimately converting the ice nanocrystals to crystalline monohydrate for the NH_3 molecule and type I clathrate hydrate for the ethylene oxide molecule. On the other hand, even though the adsorption of HCl is known to convert the ice nanocrystals to the monohydrate of HCl, the conversion is said to proceed via ionization. This is mainly due to the higher tendency of HCl to ionize in a water environment. Because they are known as “active” adsorbates, these molecules are thought to penetrate into ice, forming a solid hydrate beyond the monolayer coverage. In conjunction with those experimental investigations, theoretical studies have been carried out in order to understand the ice-adsorbate interactions. Monte Carlo simulations were performed on an ice particle $(H_2O)_{293}$ with its surface exposed to different coverages of NH_3 at 110 K [19]. At low coverage, with 16 NH_3 molecules, it was possible for the ice

surface to accommodate all NH_3 molecules since a sufficient number of dangling H-atoms of H_2O were available, and they bind in an OH- - -N fashion. At higher coverage, in addition to the strong OH- - -N bond, ammonia is inserted into the surface with the formation of additional weak NH- - -O bonds and cleavage of the H_2O- - - H_2O bonds. The behaviour of NH_3 on ice as a function of temperature was also investigated [25]. When compared to the previous work carried out by Devlin et al. [18], similar observations were made for the adsorption of NH_3 on the ice film, whereby the adsorbed ammonia molecules are in the NH_3 form. The NH_3 molecule is hydrogen bonded to the ice, H–OH- - -NH_3, and not ionic bond adsorption. However, upon annealing, the NH_3 is converted to NH_4^+ which was evidenced by the appearance of a broad peak near 1470 cm^{-1}, suggesting a proton transfer phenomenon. The latter peak was attributed to the asymmetric deformation mode of ammonium ion. Recent studies have also been done for the adsorption of polyyne, HC_5N, on amorphous ice [26]. HC_5N is one among the 130 molecules detected in interstellar clouds [26,27]. The results show that unlike other molecules studied so far, the adsorption of HC_5N does not occur through the dangling H bond because the position of the dangling H bond at 3695 cm^{-1} is found to remain unchanged during the adsorption process. However, the position of the OH stretching mode is blue-shifted during adsorption, indicating strong hydrogen bonding interaction between the HC_5N and the ice film. The authors suggested that the adsorption of HC_5N on the amorphous ice surface results in a reorganization of the surface structure. This observation was supported by the appearance of a peak at 3571 cm^{-1}, which indicates reorganization of the ice bulk.

For some time now, there has been a variety of studies involving the interaction of small molecules with ice films. Interest in the surface chemistry of ice has led to the study of adsorbed organic molecules. In our group, studies involving the surface chemistry of ice micro-phases and their interactions with acetone (a soft lewis base) have been done [28]. Adsorption of acetone resulted in the formation of a surface complex between acetone and the surface H dangling bond at a deposition pressure of $1x10^{-7}$ Torr. In particular, the acetone result demonstrates that acetone binds to the ice surface via strong hydrogen bonding between the O of the carbonyl group of acetone and H of the H-O dangling bond in the ice film. Further adsorption of acetone gave rise to a second type of complex that is bound to the surface via electrostatic and van der Waals forces. For higher exposure obtained at a higher deposition pressure ($5x10^{-7}$ Torr), multilayer formation as supported by the appearance of new IR features led us to propose the formation of a new complex closely related to the acetone clathrate-hydrate. The interaction between acetic acid and the ice surface has also been investigated by our group [29]. Acetic acid is bound to the amorphous ice surface via hydrogen bonding between the C=O group of CH_3COOH and the OH dangling bonds of the ice film. A similar observation was made for the adsorption of the same molecule on polycrystalline ice. At low exposure, the complete extinction of the OH dangling bond suggested monolayer coverage while an increasing intensity of the C=O vibration band was regarded as multilayer adsorption. More recent work on organic adsorbates includes the study of the interaction of glycine with ice nanolayers that was grown on a hydrophilic single crystalline aluminium oxide surface at 110 K and 150 K under ultra-high vacuum conditions by temperature programmed desorption (TPD) [5]. The authors concluded that

the desorption temperature of the low-temperature H_2O in the presence of glycine molecules occurs at a higher temperature as compared to desorption from pure ice layers. In correlation with the TPD measurements, X-ray photoelectron spectroscopy (XPS) and work function measurements have also been reported by the same group [30]. At 110 K, the N 1s spectra show two spectral components at 400.8 eV and 402.8 eV binding energies, corresponding to $–NH_2$ and $–NH_3^+$ groups respectively, which implies mixed adsorbed species. Upon heating the sample to 290 K, the shape and intensity of the observed N 1s spectra show no significant change. On the other hand, the O 1s XPS spectra also reveal two spectral components at 532.8 eV and 534.5 eV binding energies, attributed to the–COOH group of glycine and to H_2O, respectively.

On the basis of the literature survey carried out for the adsorption of different types of molecules on the ice surface, these species can be classified into three classes of adsorbates, based on the way they behave on an ice surface. Molecules such as CF_4, H_2, N_2 and CO are referred to as weak adsorbates because their interaction is limited solely to shift in wavenumber of the surface-localized modes. The next class of stronger adsorbates includes molecules such as HCN, SO_2, H_2S and acetylene. These molecules are known to form significant H-bonds to the OH dangling bonds of the ice surface. In so doing, they help in the reorganization of the ice structure. The last category of H-bonding adsorbates refers to molecules such as NH_3 and ethylene oxide. These species show stronger interaction with the ice surface sites, such that at higher exposures, they penetrate into the ice, resulting in amorphous or crystalline hydrates at cryogenic temperatures [31]. In spite of the extensive studies carried out so far on ice structure and the adsorption of species to its surface, the interaction of molecules of biological

importance has not been investigated. The present study deals mainly with the adsorption of simple amino acids on the ice surfaces. It should be noted that studies involving amino acids adsorbed on metal surfaces have been carried out and these results described in the next section will provide useful references for the present work.

1.4 Amino acid adsorbate

In recent times, one has witnessed a considerable interest in the adsorption behavior of amino acids on solid surfaces. The growing interest in this area has mainly been triggered by the importance of biotechnologies that involve the interaction of biological molecules with surfaces [32, 33, 34]. For instance, for the preparation of biocompatible materials, one needs to have a detailed understanding of the potential influence of these surfaces on the structure and properties of biological species [35, 36]. To be able to understand more complex systems, one has to start with simple models, and amino acids are therefore regarded as the ideal starting point. Having the general formula $NH_2CHRCOOH$ with R being the side chain, amino acids are the fundamental building blocks of proteins. Glycine is the simplest amino acid where R is a hydrogen atom. Glycine has two functional groups that are common to all amino acids, the amino group (NH_2) and the carboxylic group (COOH). This simplest amino acid lacks an important property present in other amino acids, namely chirality. This important phenomenon occurs when R is not the H atom and the molecule could then exist in two distinct forms or enantiomers that are mirror images to each other. Alanine is thus considered as the smallest chiral amino acid with R being the methyl group, CH_3. At room temperature, glycine exists as a crystalline solid in the zwitterionic form ($NH_3^+–CH_2–COO^–$), in which a proton is

transferred from the carboxylic to the amine group [33]. In the solution phase, the zwitterionic form also predominates, whereas in the gas phase glycine is present in its neutral form (NH_2–CH_2–COOH). Moreover, in acidic or basic solution, the zwitterions could gain or lose protons, resulting in the cationic (NH_3^+–CH_2–COOH) or anionic (NH_2–CH_2–COO^-) form of glycine, respectively. Similar characteristics are attributed to the simplest chiral amino acid, alanine, which will also be examined in the present work. An interesting feature of the neutral molecule glycine is that it can exist in three distinct polymorphic forms, namely α, β and γ glycine, with the γ–glycine being the most stable form at room temperature [33, 37]. The γ–glycine structure consists of helical chains of roughly parallel head-to-tail glycine molecules. These chains are hexagonally packed via lateral hydrogen bonds. On the other hand, alanine molecule exhibits two enantiomeric forms, the L and D forms, because of the stereoasymmetry α-carbon atom present in that species [7]. Life on Earth is based on the L-amino acids [38]. However, the D-form can be found in some scarce bacterial amino acids and in some amino acids making up the proteins of amphibian skin [7].

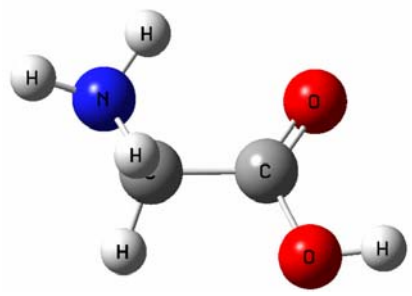

Figure 1.4: Structure of glycine.

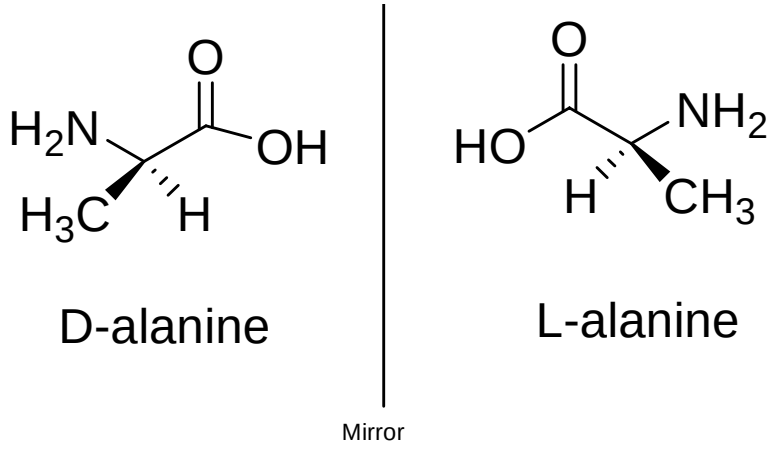

Figure 1.5: The two optical isomers of alanine, the D- (left) and L-alanine (right).

1.5 Adsorption of amino acids on metal surfaces

The interaction of biological molecules with solid surfaces is of considerable interest because of its importance in the studies of the biocompatibility of artificial implants in living systems, biocorrosion, and other technologies [35, 39]. In order to be able to understand how complex systems interact with surfaces, glycine and alanine amino acids are seen as good testing grounds to develop better understanding of how H-bonds, present in biological systems, are altered in the presence of a metal surface [40]. Earlier studies include the infrared and photoelectron spectroscopy of amino acids adsorbed on copper [41]. Copper films were prepared by thermal evaporation with three different evaporation rates; 5, 40 and 90 Å/s, were used. Transmission electron microscopy (TEM) was used for characterization of the copper film, and the results show that copper films obtained at 5 and 90 Å/s evaporation rates are closely related to the (111) orientation while the one at 40 Å/s has more of a polycrystalline character [41]. Adsorption of glycine on the Cu(111) surface did not produce any peaks in the 3200-2300 cm^{-1} region, which corresponds to the intermolecular hydrogen bonding $–NH_3^+ - - - - {}^-OOC–$ in the crystalline species [41].

This suggests that the zwitterionic character appears to be disrupted during adsorption. The absence of the band at 1524 cm^{-1}, assigned to the symmetric NH_3^+ deformation mode, confirmed the aforementioned observation. This leads to the assumption that the nitrogen of the amino group of glycine molecule is involved in the bonding to the metal. However, because both COO^- asymmetric stretching and NH_2 scissoring modes occur in the 1550–1650 cm^{-1} region, it was difficult to assign these peaks. Glycine adsorption on a Cu(110) surface at 300 K has been studied by Barlow et al. using reflection-absorption infrared spectroscopy (RAIRS) [36]. These authors observed that at room temperature, glycine forms a saturated monolayer on the Cu(110) surface. This was demonstrated by the evolution of the RAIRS spectra until a saturated surface was formed whereby no further glycine adsorption was found to occur. The most interesting aspect of the RAIRS data was the absence of the carbonyl stretching band near 1720 cm^{-1}, which indicated that the adsorbed glycine has an ionic character rather than an acid form. This was confirmed by the presence of the peak at 1417 cm^{-1}, assigned to the COO^- symmetric stretching vibration, at low coverage. However, due to the intermixing of local modes, it is difficult to distinguish between the NH_2 and NH_3^+ IR peaks. At higher coverage, the orientation of the glycine species on the Cu(110) surface has altered, such that an overall bidentate species was observed, based on the RAIRS data, while the authors concluded that glycine binds to the surface in a tridentate fashion at low coverage. Low-temperature experiments (with the Cu substrate held at 85 K) indicated that glycine remains as the acid form, evidenced by the carbonyl stretching peak at ~1720 cm^{-1}. The carbonyl stretching peak which consequently disappears upon warming the surface, suggesting that glycine is converted to its zwitterionic form. Low-temperature experiments give rise to multilayer

formation where the intensities of the bands continue to increase with increased exposure. Efstathiou and Woodruff investigated the adsorption of glycine on Cu(100) and Cu(111) [33]. The RAIRS data showed that glycine adsorption on Cu(100) and Cu(111) is similar to that on Cu(110). In all three cases, the glycinate species were observed. Moreover, tridentate and bidentate species were obtained at low and high coverages, respectively, on the Cu(100) and Cu(111) surfaces.

Besides Cu surfaces, characterization of the interaction of glycine on other types of surfaces has also been studied. For instance, Löfgren obtained TPD and XPS results for glycine deposited on Pt(111) [42]. The XPS results reveal a zwitterionic species adsorbed on Pt(111), with two C 1s peaks, related to the α-C and to the deprotonated carboxyl group, two N 1s peaks [with the dominating one being associated to the protonated amino group (NH_3^+) and the very weak one to the neutral amino group (NH_2)] and one O 1s peak, related to the deprotonated carboxyl group. In conjunction with the XPS results, the TPD data confirm molecular adsorption of glycine species [42]. This was explained by the desorption temperatures observed for the different fragments. Had there been dissociation upon adsorption, desorption of the dissociation products would have occurred at much lower temperatures, but this was not the case. The IR spectra for glycine deposited from the vapour onto a CsI substrate at 9 K has been presented by Gomez-Zavaglia and Fausto [43]. Two different evaporation temperatures, namely 87 and 64 °C, were used. The authors noted that glycine deposited at low temperature occurs in a mixture of neutral and zwitterionic forms of the glycine species and that the neutral glycine exists as aggregated species. The latter observation was explained by the positions of the bands corresponding to O–H stretching, NH_2 asymmetric stretching, NH_2

symmetric stretching and C=O stretching modes that appeared at lower wavenumbers compared to those for the monomer. Moreover, the authors showed that the bands associated with the neutral species were more intense for the deposition at 64 °C sublimation temperature. This was explained in terms of the local heating effects. As the hot glycine molecules land on the cold CsI surface the thermal energy can be used to induce the proton transfer, transforming the neutral species into the zwitterionic form.

Adsorption of L-alanine on Cu(110) surface was found to follow a similar behavior as glycine adsorbed on Cu(110) [44]. Williams et al. showed that the alaninate species predominates at 300 K on the Cu(110) surface. Two species were basically observed, one at low coverage, where the carboxylate oxygen atoms were found to be equidistant to the metal surface, while for the high coverage, the COO^- showed a sideway-tilted orientation with only one oxygen atom of the carboxylate group binding to the surface. These observations are similar to those obtained as in the case of glycine [33, 35, 36, 39, 41, 42]. Furthermore, Iwai et al. reported the scanning tunneling microscopic (STM) study of the adsorption of D-alanine on Cu(100) [45]. The STM data revealed that the adsorption occurs in a similar fashion to that of glycine on Cu(100) because similar arrayed structures were observed, with the occurrence of the alaninate species on the surface.

1.6 Objectives of this work

In the present work we present the RAIRS results for the adsorption of glycine and alanine molecules on both non-crystalline ice (NCI) and polycrystalline ice (PCI) as well as the polycrystalline Cu support held at room temperature as well as low temperature.

The thermal evolution of the adsorbed species on the NCI and PCI surfaces is investigated by following the RAIRS data upon successive annealing of the as-deposited sample. These studies will provide new insights to the following questions:

- How do the amino acids bind in general to the surface? Is the bonding non-dissociative or dissociative? What is the role of hydrogen bonding?
- Where and how are the molecule-surface bonds established (at the amine group, and/or at the carboxylic group, and/or at the R-side group etc.)? How important is site-specific chemistry on ice?
- Molecular orientations on ice and their connections to molecular chirality.
- To what extent does the ice surface catalyze polymerization (e.g. forming peptide bonds)?

To the best of our knowledge, the present work represents the first such study of amino acids on ice using the RAIRS technique.

Chapter 2

Experimental Details

The present study was carried out in a home-built ultra-high vacuum (UHV) system, shown in Figure 2.1, with a base pressure better than 3 x 10^{-9} Torr, achieved by a 180 L/s BALZER TPH turbomolecular pump and a titanium sublimation pump. The pressure shown in Figure 2.1 is obtained when the sample is cooled to 125 K. The system is equipped with ion-sputtering and sample heating facilities for sample cleaning. The UHV system also consists of a Bruker Equinox 55 Fourier Transform Infrared spectrometer for RAIRS experiments and a quadrupole mass spectrometer for TPD measurements.

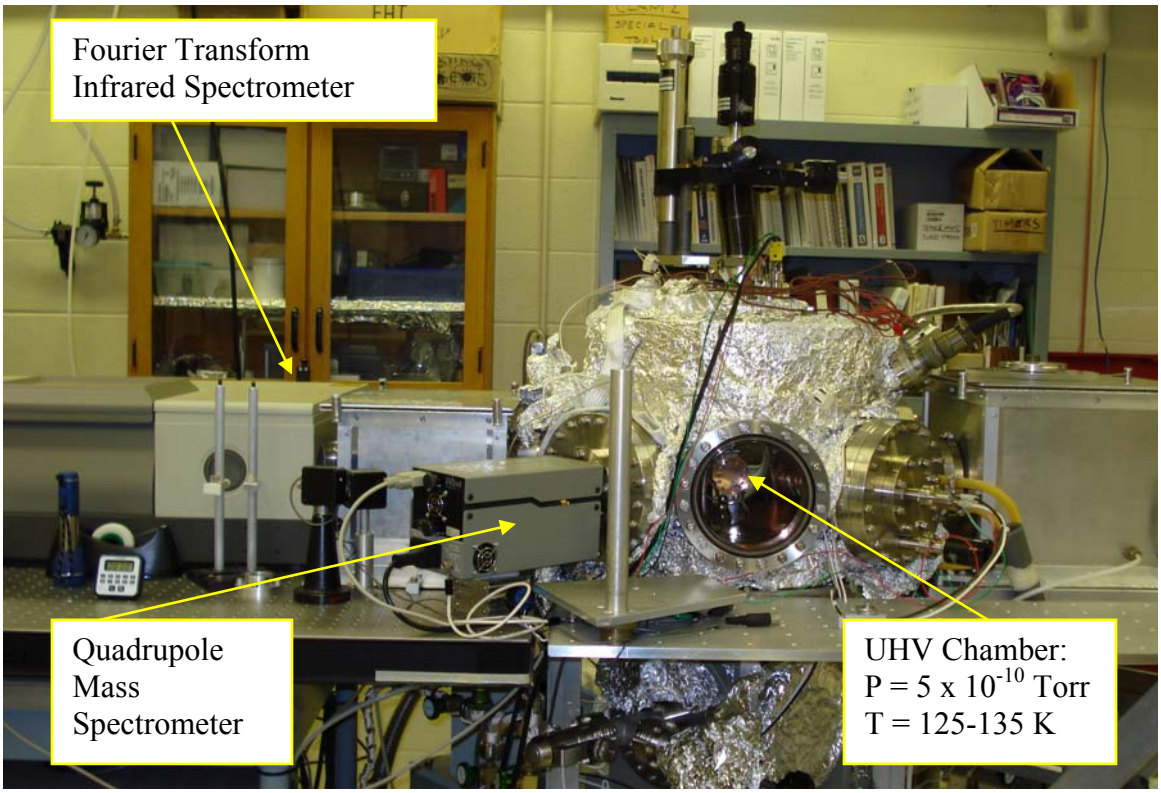

Figure 2.1: Experimental set-up

In the present work, a vertically mounted, optically flat polycrystalline copper substrate (5.7 cm in diameter), shown in Figure 2.2, was used for film growth by vapor deposition. The polycrystalline copper support was attached to a liquid nitrogen-cooled dewar and the temperature was measured using a K-type thermocouple fastened to the front of the disk. After cooling the Cu disk, the base pressure inside the UHV chamber was in the 10^{-10} range. The substrate could also be annealed to a higher temperature by a resistive heater embedded in the backside of the Cu disk under the control of a temperature controller [11]. Prior to vapour deposition, an important consideration in the field of surface modification is the cleanliness of the surface. The Cu disk was cleaned by several cycles of Ar ion bombardment at 1.5 kV for 30 minutes in order to ensure a surface free of contaminants. During the argon sputtering experiment, the argon gas pressure was kept at 1.0×10^{-5} Torr.

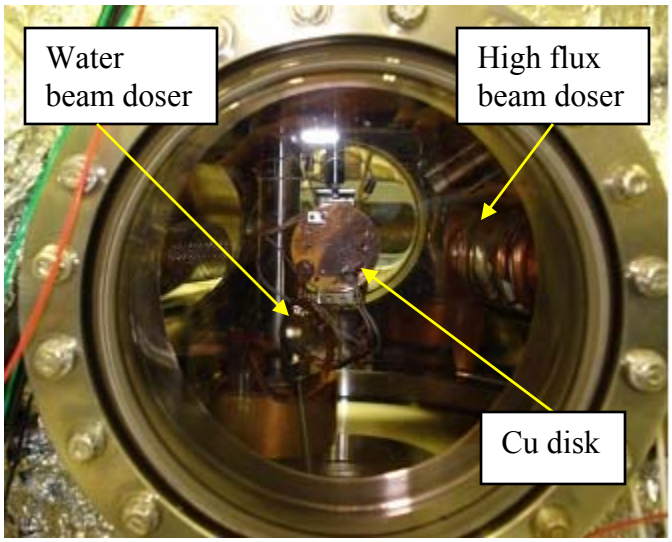

Figure 2.2: Cu disk, water beam doser and high flux beam doser inside the UHV chamber.

The chamber also contains a beam doser for introduction of water vapour, shown in Figure 2.2. Deposition of the ice films was carried out by introducing vapours of water (Millipore) in the UHV chamber through a variable precision leak valve. For the deposition of non-crystalline ice and polycrystalline ice films, the Cu disk was kept either at 123 K or 155 K, and the chamber was filled with water vapour at a pressure of 15 nTorr (1 nTorr = 1 x 10^{-9} Torr) for a predetermined deposition time. Deposition times varied from about 20 minutes for the NCI and 30 minutes for the PCI. It is necessary to freeze-pump-thaw the liquid water sample several times prior to use in order to remove dissolved oxygen and other gases.

A specially designed cryogenic effusive cell was used in the present work to evaporate the amino acids. The effusive cell utilized in the present work consisted of a crucible, which contained the amino acid, heating filaments (made of tantalum wires), liquid nitrogen cooling system, heat shields and a shutter. The high-flux beam, shown in Figure 2.3, was built in the group by Dr. Michel Mallick Thiam. The amino acid was initially outgassed at 373 K for several hours, with the shutter closed, before evaporation. It was imperative to first determine the appropriate evaporation temperature of the amino acids, without thermally cracking the compounds. Glycine and alanine were evaporated at 446 and 453 K respectively. During dosing, the amino acid was heated to the appropriate temperature and the substrate was positioned facing the doser with its shutter opened.

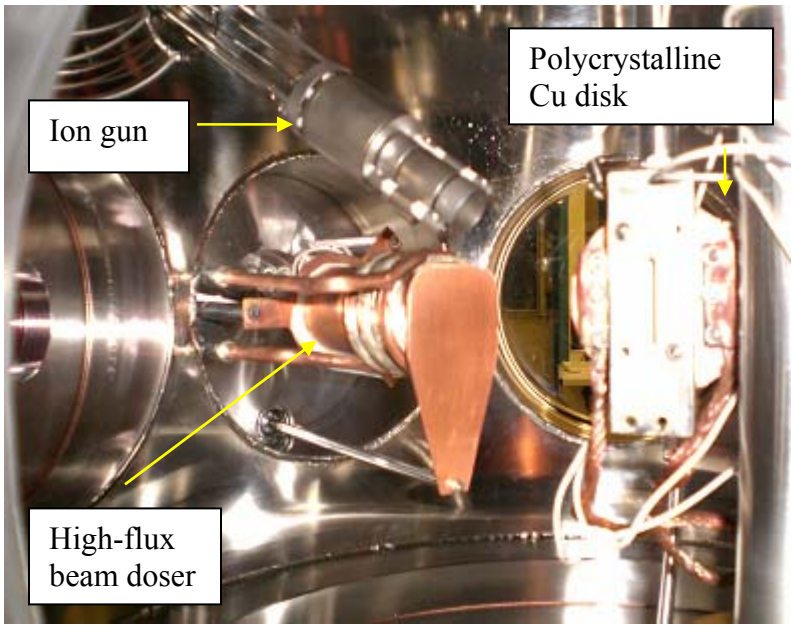

Figure 2.3: A high-flux beam doser with cryogenic shielding (Photo taken from the back side of the Cu disk).

The FTIR unit used was a Bruker Equinox 55 Fourier transform infrared spectrometer. The RAIRS spectra were recorded over a spectral range of 4000-650 cm^{-1} using a liquid-nitrogen-cooled mercury-cadmium-telluride (MCT) detector and a KBr beamsplitter, and were collected with a spectral resolution of 4 cm^{-1}. Each sample spectrum consisted of 250 scans while the background spectra were collected for the bare copper disk at the deposition temperature. The clean surface background consisted of 500 scans. The resulting background-subtracted sample spectra were then given in the dimensionless absorbance unit, defined as $-\log (R/R_0)$, where R/R_0 is the ratio of the reflectance of the substrate with and without the adsorbate. Figure 2.4 shows schematically the glancing–incidence optical arrangement of the experimental set-up.

The IR beam was directed first on a flat mirror at 45° followed by a 90° refocusing parabolic mirror, enclosed in an aluminium box on the left side of the chamber, and finally to the Cu disk at 83° from the surface normal. The reflected beam was collected by an identical parabolic mirror on the opposite side of the chamber, and ultimately focused on the mercury-cadmium-telluride detector by another smaller parabolic mirror. Two KRS-5 (Thallium Bromoiodide) optical windows were used to provide passage of the IR beam onto the sample inside the UHV chamber. The He-Ne laser and the detector shown in Figure 2.4 were not used in the present studies. The entire optical path was purged with dry nitrogen gas in order to remove spectral interference due to ambient water vapour and carbon dioxide.

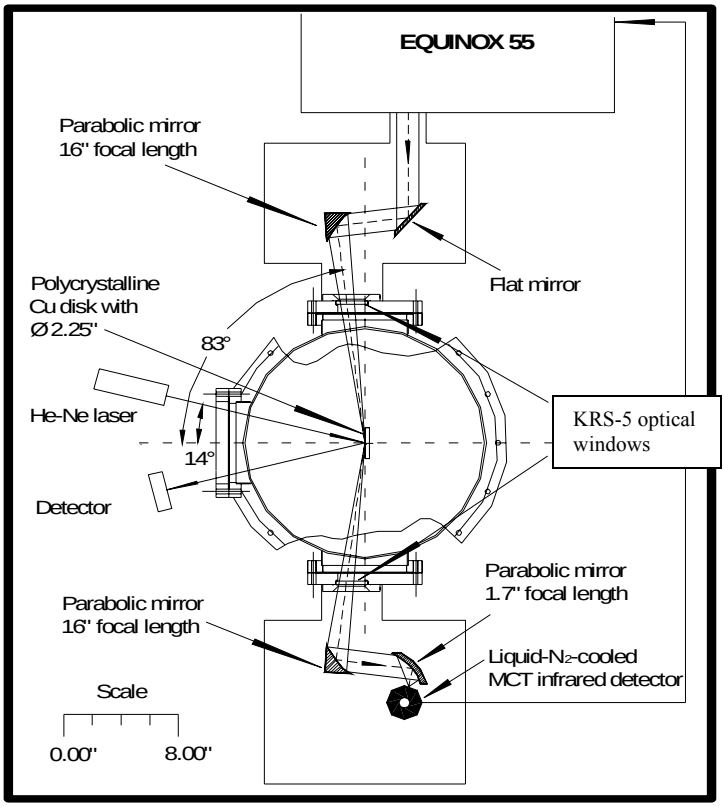

Figure 2.4: Schematic layout of the optical arrangement of a reflection-absorption apparatus [11].

2.1 Experimental procedure

A polycrystalline Cu disk was used for the experiments. Prior to all experiments, the Cu disk was cleaned by cycles of Ar^+ sputtering. Following the cleaning procedure, the Cu support was cooled to ~120 K. The typical base pressure following such a procedure was ~5 x 10^{-10} Torr. After the Cu support was cooled to ~120 K, the background spectrum was recorded for the bare Cu surface, consisting of 500 scans and took approximately 2 minutes to acquire. Following acquisition of the background spectrum, the Cu disk was exposed to water vapour at a pressure of 1.5 x 10^{-8} Torr for 20 to 30 minutes, depending on the experiment. The relative exposure time was 20 and 30 minutes for NCI and PCI film, respectively. Subsequent spectra for the NCI film were recorded in real time, and typically 250 scans were taken resulting in collection of a full spectrum in about 1 minute. Once the NCI film is obtained, the sample is heated at a heating rate of 0.04 K/s to 160 K, in order to induce transformation of the NCI to PCI film. The amino acid powder was contained in a small crucible inside the high-flux beam doser. The crucible was heated to a temperature 446 K for glycine and 453 K for alanine, and the amino acids exposed to the NCI and PCI films for 15 minutes. During exposure, the main chamber pressure was in the 10^{-8} range. RAIRS spectra were collected for the sample at the same time. Following exposure of glycine and alanine to the NCI and PCI films, thermally induced desorption experiments were carried out using a heating rate of 0.04 K/s while acquiring the RAIRS spectra.

Chapter 3

Results and Discussion

3.1 RAIRS spectra of non-crystalline and polycrystalline ice films

Vibrational spectra recorded in the present work for the two types of ice formed between 123 and 160 K are now discussed. Figure 3.1 compares the RAIRS spectra of a non-crystalline ice (NCI) film deposited at 1.5 x 10^{-8} Torr for 1200 s on a polycrystalline copper disk held at 123 K, and a resulting polycrystalline ice (PCI) film formed after annealing to 160 K. The infrared spectrum of the NCI film [Figure 3.1(a)] is characterized by a broad, strong peak near 3400 cm^{-1}, which can be identified with the stretching modes of the hydrogen-bonded OH bonds, and by weaker bands in the lower wavenumber region. The peaks at 1678 cm^{-1} and 895 cm^{-1} are assigned to the H-O-H bending and to librational modes, respectively, while the weakest feature at 2228 cm^{-1} corresponds to the combination band. It is associated with the combination of the overtones of the translational and rotational lattice modes with the fundamental bending mode at 1678 cm^{-1} [46]. The weak but relatively sharp peak at 3695 cm^{-1} is reported as the free dangling OH bond of surface H_2O molecules that do not participate in the hydrogen-bonding network [47]. These spectral assignments are in accordance with the previous work on ice [6, 9–31]. Figure 3.1(b) shows a typical spectrum of a PCI film, which is obtained after annealing the NCI film at a constant rate of 0.04 K/s to 160 K. A slow heating rate (0.04 K/s) was used in order to prevent the ice film from desorbing before any transformation occurs because the non-crystalline to polycrystalline transformation and desorption of the NCI occur in the same temperature range. Annealing the NCI film caused a drastic change in the band shape in the 3600-3000 cm^{-1}

region. Figure 3.2 shows the evolution of the RAIRS spectra for the coupled OH stretch mode during the annealing. The observed spectra are consistent with earlier studies [9, 11–14, 20, 28, 29]. In particular, the intensities of the bands differ from one spectrum to the other, particularly for the intensities of the OH stretching band, bending mode and librational mode. The considerable reduction in intensity of the dangling OH band featuring at 3695 cm^{-1} for the NCI film to 3692 cm^{-1} for the PCI film (Figure 3.1, Inset) is an indication that the dangling OH bonds have become more orientationaly disordered. The increasing surface disordering with temperature suggests that the melted surface layer becomes liquid-like [6]. Moreover, the shift in the OH stretching band towards lower wavenumber confirms the crystalline state of the ice film, reflecting an increase in structural ordering of the ice film.

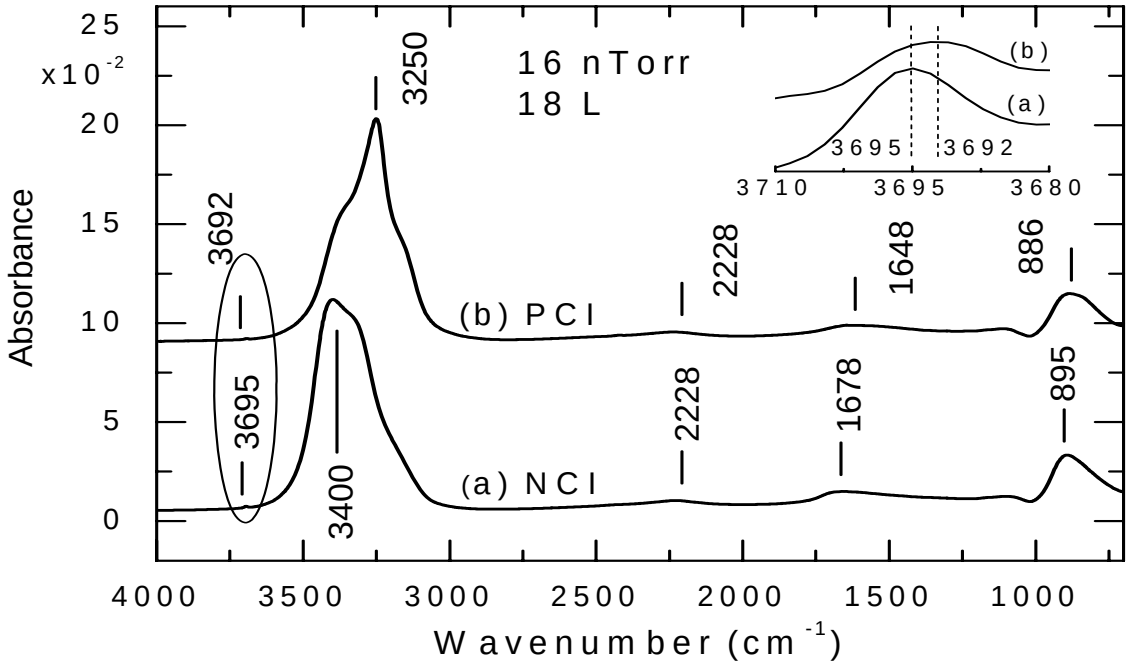

Figure 3.1: Comparison of the RAIRS spectra of (a) non-crystalline ice (NCI) and (b) polycrystalline ice (PCI) films on Cu support obtained at a deposition pressure of 16 nTorr for 18 L (1 L = 1 x 10^{-6} Torr s). Inset shows the dangling OH bond region.

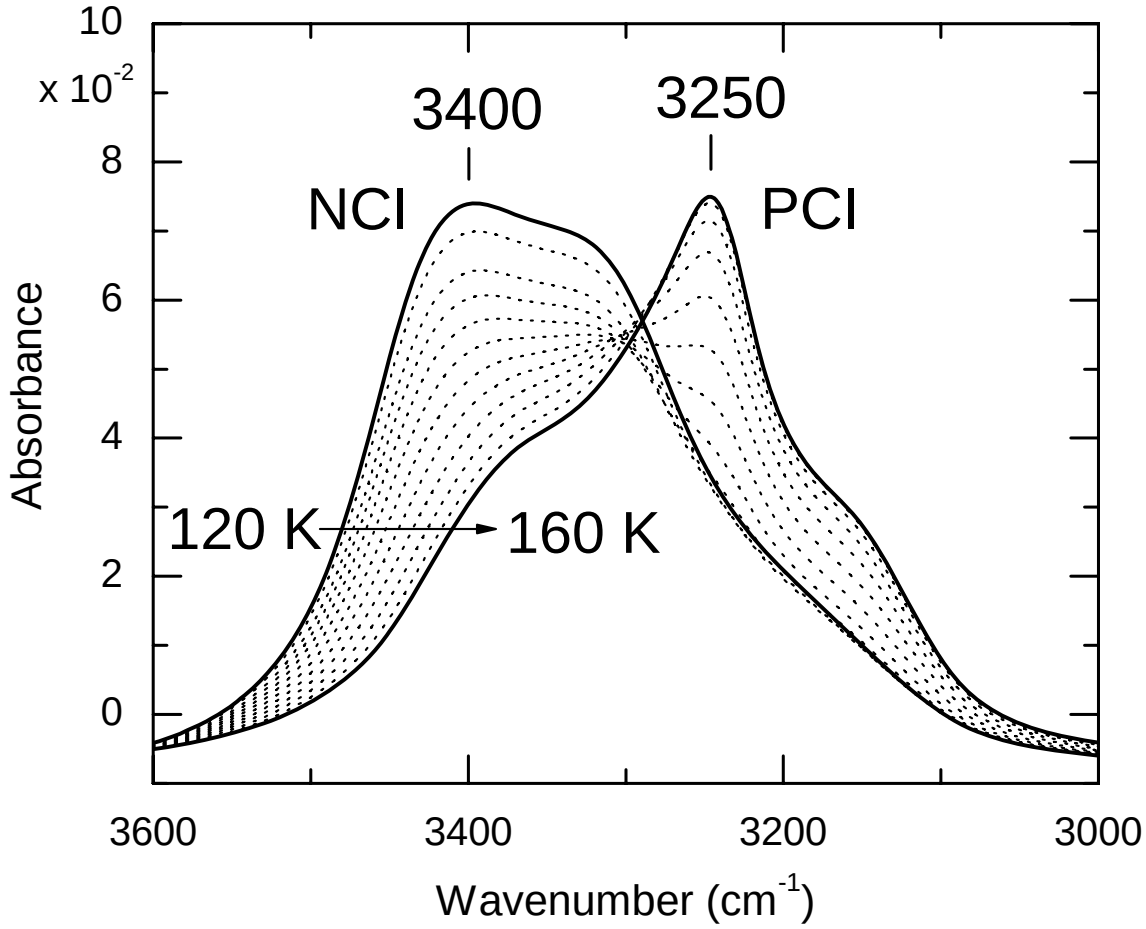

Figure 3.2: Evolution of the OH stretching mode during annealing of a non-crystalline ice (NCI) film to a polycrystalline ice (PCI) film.

3.2 Adsorption of glycine on polycrystalline Cu at two different temperatures

The FTIR spectra for glycine deposited on a polycrystalline copper surface at 121 K are illustrated in Figures 3.3 and 3.4, while the corresponding spectra collected at room temperature are shown in Figure 3.5. In order to have a better understanding of the underlying adsorption process, the collected data have been divided into the low-exposure and high-exposure sets, given by Figures 3.3 and 3.4 respectively. Since the

glycine molecule contains the amino and carboxyl groups, these functional groups are expected to be the sites at which adsorption occurs and therefore particular attention is paid to the regions where these functional groups appear. Table 3.1 compares the vibrational wavenumbers observed for glycine deposited on the polycrystalline Cu surface at low and room temperature. With reference to the data published for glycine adsorption on different metal surfaces [33, 36, 39, 41, 43], the assignments for the most prominent bands are given in Table 3.1. From the initial stage of adsorption, few peaks appear in the low wavenumber region and these are 1730, 1568, 1430 and 1240 cm^{-1} at 0.18 L exposure [Figure 3.3(a)]. It is difficult to determine with certainty the corresponding assignments for these peaks at the very beginning of exposure due to the intermixing of modes for the glycine species. However, with further exposure to 0.60 L [Figure 3.3(b)] and 1.26 L [Figure 3.3(c)], the peaks become more distinguishable. In order to be able to interpret the RAIRS data, the direction of the dipole moment associated with each vibration should be considered since only those surface vibrations with dipole moments perpendicular to the surface could be observed according to the surface selection rule [28, 36, 41]. For instance, the band at 1730 cm^{-1} appearing as a small peak in Figure 3.3(a) may be confidently assigned to the C=O stretching vibration of the –COOH group of the glycine species, which immediately suggests that the glycine molecule is adsorbed in its neutral –COOH acidic form, in good accord with the previous work [36, 43]. Figure 3.3(b) illustrates the growth of additional spectral features with further glycine adsorption. For a 0.60 L exposure, the band at 1568 cm^{-1} is found to split into two components at 1658 cm^{-1} and 1576 cm^{-1} with the former being higher in intensity. Moreover, the band at 1430 cm^{-1} also evolves in two different peaks at 1437

cm^{-1} and 1405 cm^{-1} nearly equal intensity. On the other hand, no significant changes besides an increase in intensity can be seen for the peak at 1240 cm^{-1}, which appears to grow as a singlet with further exposure. Further changes are observed at 1.26 L exposure [Figure 3.3 (c)], whereby the band at 1568 cm^{-1} undergoes a blue shift to 1601 cm^{-1}. It can also be seen that the peaks at 1658 cm^{-1} and 1601 cm^{-1} have almost the same intensities. A blue shift of 7 cm^{-1} is also observed for the feature appearing at 1430 cm^{-1}. It should be noted that the latter band is dominated by the peak located at 1405 cm^{-1}. A new feature appears at 1322 cm^{-1} for the 1.26 L exposure and this can be attributed to CH_2 wagging vibration. The emergence of new peaks with increasing exposure suggests that the glycine molecules re-orientate themselves. The absence of some features at 0.18 L exposure implies that these vibrational modes likely had their dipole moments parallel to the surface and thus were infrared inactive. It should be noted that both the position and the intensity of the peak at 1730 cm^{-1} are modified with coverage, producing a red-shift of 6 cm^{-1} for the 0.60 L and 14 cm^{-1} for the 1.26 L exposure. These observed changes indicate a strong influence of the orientation of the adsorbate on the cold Cu substrate at different coverage. Considering the high wavenumber region, new spectral features appear at 2957 cm^{-1} and 2914 cm^{-1}, which are associated with CH_2 asymmetric and CH_2 symmetric stretching vibrations respectively for the 1.26 L coverage.

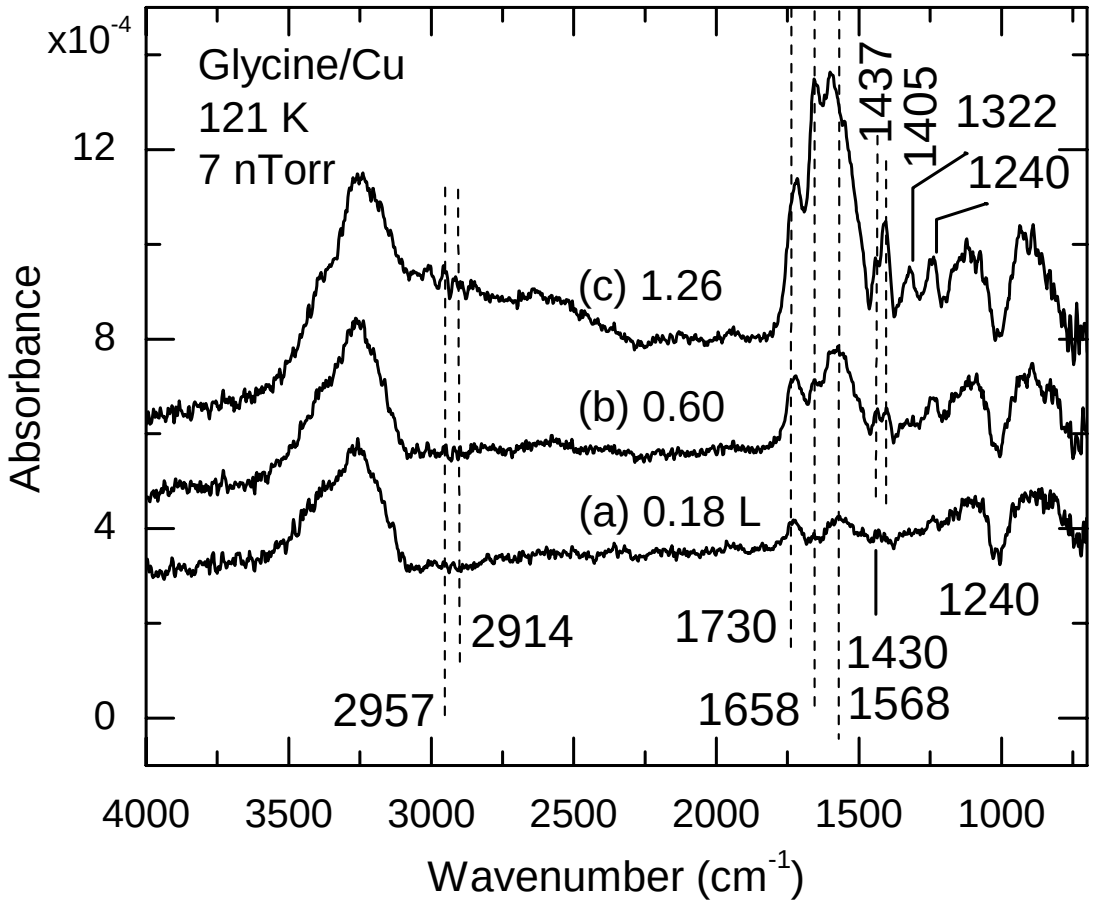

Figure 3.3: RAIRS spectra of (a) 0.18 L, (b) 0.60 L, and (c) 1.26 L of glycine deposited on polycrystalline Cu at 121 K.

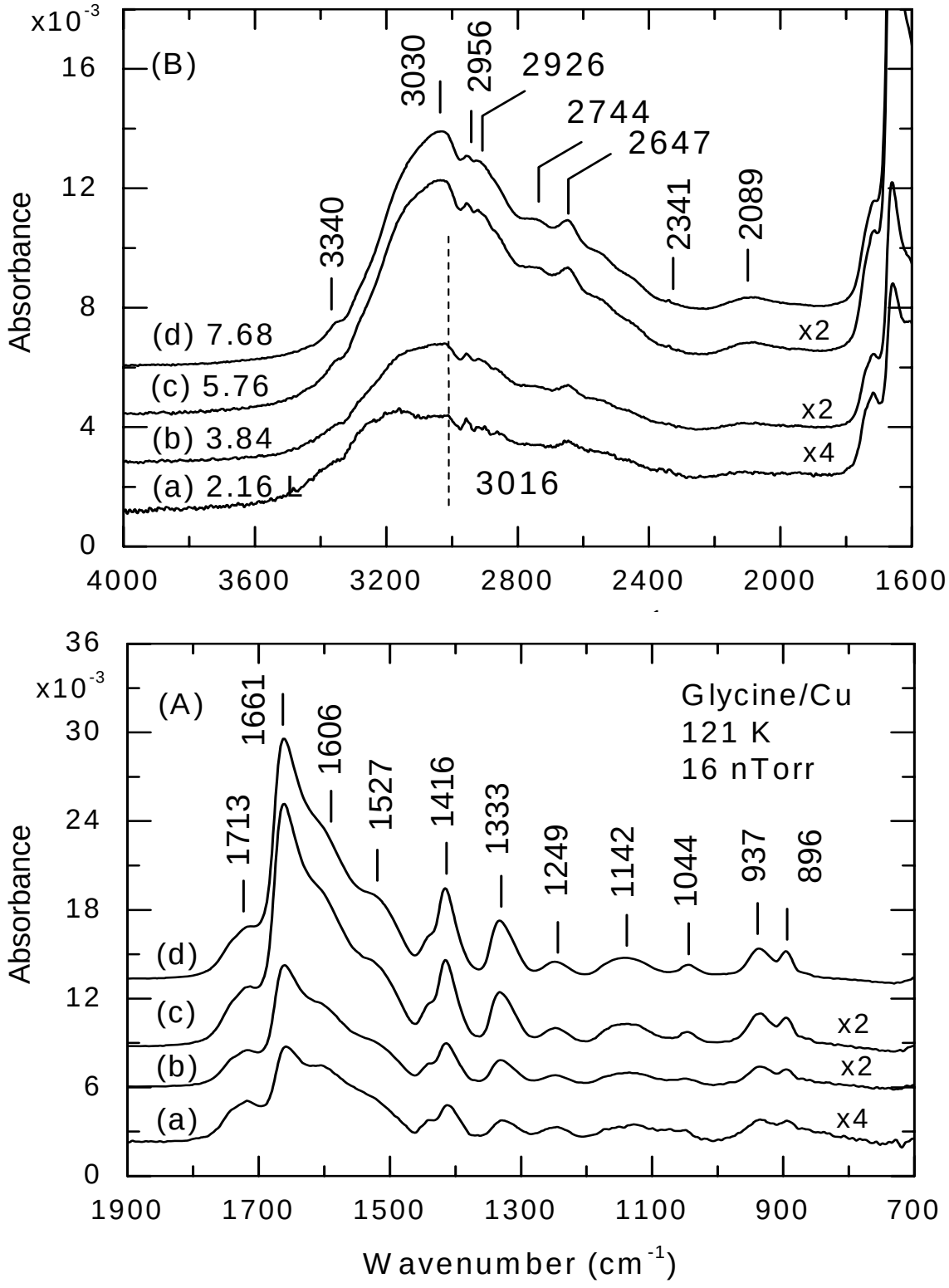

Figure 3.4: RAIRS spectra of (a) 2.16 L, (b) 3.84 L, (c) 5.76 L, and (d) 7.68 L of glycine deposited on polycrystalline Cu at 121 K.

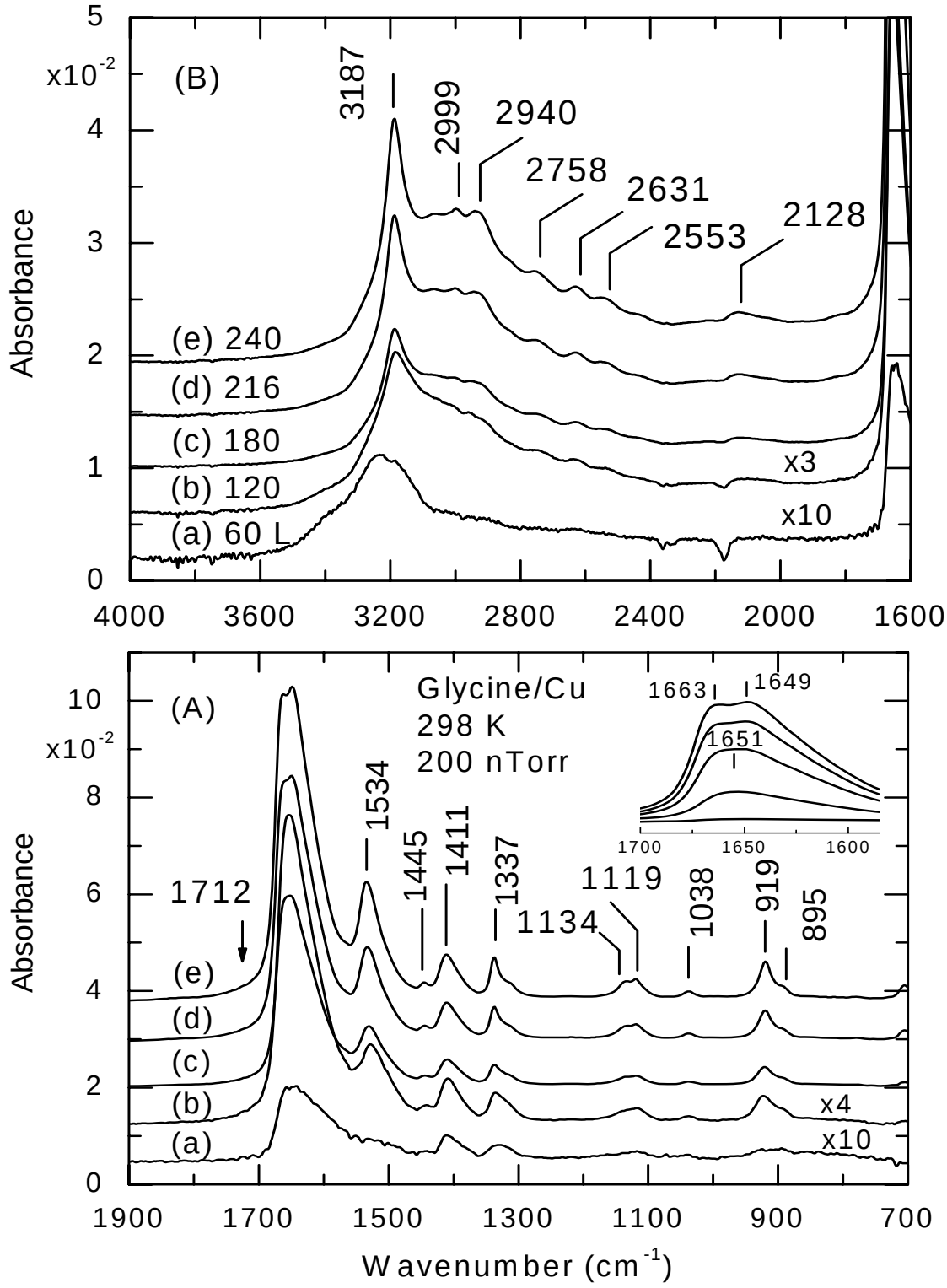

Figure 3.5: RAIRS spectra of (a) 60 L, (b) 120 L, (c) 180 L, (d) 216 L, and (e) 240 L of glycine deposited on polycrystalline Cu at 298 K.

In order to more comprehensively analyze the evolution of the infrared spectra for the adsorbate as a function of exposure, the RAIRS data have been divided into the low-wavenumber and high-wavenumber regions in Figure 3.4. Compared to the 1.26 L exposure [Figure 3.3(c)], it is clear that the 2.16 L exposure produces a different orientation of the adsorbed species, and this is evidenced by the peaks in the 1900-700 cm^{-1} region. At 0.60 L coverage, the feature at 1568 cm^{-1} dominates but growth of this band at 1606 cm^{-1} soon ceases for the 2.16 L coverage. Instead there is very rapid growth of the peak at 1661 cm^{-1}, which shows a blue-shift on further exposure and is identified as the NH_2 scissoring mode. A similar observation can be made for the peak at 1437 cm^{-1}, which shows no significant change, while the peak at 1405 cm^{-1} for the 0.60 L coverage has now shifted to 1416 cm^{-1} for the 2.16 L coverage and dominates the former band. The latter can be associated with the COH scissoring and CO stretching vibrations [43]. The remaining bands attributable to the neutral form of glycine are 1333, 1249, 1142, 1044, 937 and 896cm^{-1} for the low-wavenumber region [Figure 3.4 (A)] and the corresponding assignments are given in Table 3.1. As the surface is further exposed to glycine, the absorption bands continue to increase in intensity, suggesting multilayer coverage [36]. The appearance of the band at 3016 cm^{-1} also suggests multilayer formation. It is interesting to observe the changes occurring in the high-wavenumber region as well, illustrated in Figure 3.4 (B). Both the peaks at 2956 cm^{-1} and 2626 cm^{-1} increase in intensity, while a new band at 3016 cm^{-1} starts growing at 2.16 L. The latter band increases drastically at 5.76 L, and is shifted to 3030 cm^{-1} wavenumber. Based on the previous work carried out by Barlow at al. [36], the broad band at 3030 cm^{-1} can be

regarded as intermolecular hydrogen bonding between the glycine molecules in the multilayers.

In comparison to the study of glycine on polycrystalline Cu at low temperature, the room-temperature experiment reveals similarities as well as differences in the RAIRS spectra. Figure 3.5 shows the evolution of the RAIRS spectra with increasing glycine exposure at room temperature. In particular, the absence of the C=O stretching band near 1700 cm^{-1} [marked by the arrow in Figure 3.5 (A)] indicates that the glycine species adsorbed as an anionic species at room temperature. This is confirmed by the presence of the COO^- asymmetric stretching vibration at 1658 cm^{-1} at an early stage of adsorption, which dominates the RAIRS spectra. The next obvious difference observed between the low-temperature (Figure 3.4) and room-temperature spectra (Figure 3.5) is the peak at 1534 cm^{-1} for the room temperature data, but which is seen as a shoulder for the low-temperature experiment. Ihs at al. [41] showed that a peak arising at 1524 cm^{-1} is associated with the NH_3^+ symmetric deformation mode for a glycine KBr pellet. Solid glycine exists in the zwitterionic form. Barlow at al. [36] also attributed the a peak at 1533 cm^{-1} to the NH_3^+ symmetric deformation mode, reflecting a zwitterionic character. Moreover, Carlsson and Liedberg observed the strong NH_3^+ symmetric deformation band at 1528 cm^{-1} [48]. However, recent studies carried out by Efstathiou and Woodruff suggested that the peak appearing at ~1580 cm^{-1} is associated with the NH_2 scissoring mode [33]. On the basis of literature, we may suggest that the 1534 cm^{-1} has more of a zwitterionic character and is related to the NH_3^+ asymmetric stretching mode. Moreover, the 1416 cm^{-1} band, related to the combination of the CO stretching and COH bending modes, occurs at a lower wavenumber (1411 cm^{-1}) with a lower intensity. The band at

1411 cm^{-1} is assigned to the COO^- symmetric stretching vibration for the room-temperature experiment.

It is interesting to note that the bands at 1411 and 1337 cm^{-1} have approximately the same intensities for the 240 L exposure [Figure 3.5(B)(e)] in contrast to the low temperature experiment (Figure 3.4). This may be indicative of a change in orientation. Notice that at room temperature, the peak at 1249 cm^{-1}, assigned to CO stretching and COH bending modes, is absent [Figure 3.5(A)]. This may be explained in terms of the surface selection rule, which states that only modes having a dipole moment perpendicular to the metal surfaces are observable [36]. The fact that the peak at 1249 cm^{-1} was seen earlier for the low-temperature experiment can be thought as the vibrational mode at 1249 cm^{-1} having a component of the transition dipole moment perpendicular to the metal surface and therefore appearing in the RAIRS spectra. This confirms the fact that at room temperature, deprotonation at the –COOH group occurs, causing the absence of the peak at 1249 cm^{-1}. In addition, a sharp peak at 919 cm^{-1}, with a weaker peak at 895 cm^{-1} are seen for the room-temperature spectra while two distinguishable peaks of approximately the same intensity are seen at 937 and 896 cm^{-1} for the low-temperature spectra. The peak at 919 cm^{-1} is assigned to the CH_2 rocking mode whereas the band at 895 cm^{-1} is attributed to CC stretching mode. It should be noted that both red and blue shifts are observed in the 4000–700 cm^{-1} region when the room-temperature and low-temperature experiments are compared. Of particular interest is the sharp peak at 3187 cm^{-1} [shown in Figure 3.5 (B)], which is not seen for the low-temperature spectra. A peak occurring at 3169 cm^{-1} was assigned to the NH_3^+ asymmetric stretching mode for the glycine KBr pellet [41]. Moreover, a band at 3152 cm^{-1} is

associated with zwitterionic characacter [36]. Thus, it seems reasonable to say that at room temperature, the zwitterionic structure of glycine is predominant, as confirmed by the peak at 3187 cm^{-1} that originates at 120 L exposure [Figure 3.5 (B)] and continues to grow at higher exposure. The nitrogen of the NH_3^+ group may be involved in bonding to the metal. Apart from the evidence of orientational changes for the 121 K and 298 K experiments, there is another point that is worth mentioning. Notice that up to 180 L exposure, the peak at 1651 cm^{-1}, assigned to COO^- asymmetric stretching mode, appears as a singlet. However, a splitting of the 1651 cm^{-1} peak into two components at 1663 and 1649 cm^{-1} occurs for the 216 L exposure, shown as an inset in Figure 3.5 (A). It is not clear why splitting occurs at this stage. From these observations, we may conclude that glycine remains as the acid –COOH (with the group intact) as it is deposited at 121 K, while it is difficult to say whether the NH_2 or NH_3^+ group is present. Noteworthy at 298 K, the zwitterionic form predominates. Moreover, multilayer formation occurs at 121 K, evidenced by the band at 3030 cm^{-1}.

Table 3.1: Assignments of experimental infrared bands of glycine evaporated on polycrystalline Cu at 121 K and 298 K.

Glycine/Cu at 121 K		Glycine/Cu at 298 K	
Vibrational mode	Wavenumber (cm^{-1}) [Ref. 43]	Vibrational mode	Wavenumber (cm^{-1}) [Refs 36, 41]
ν_{as} (CH_2)	2956	ν_{as} (NH_3^+)	3187
ν_s (CH_2)	2926	ν_{as} (CH_2)	2999
ν (C=O)	1713	ν_s (CH_2)	2940
δ (NH_2)	1661	ν_{as} (COO^-)	1651
δ (COH) + ν (CO)	1416	δ_s (NH_3^+)	1534

ω (CH_2)	1333	δ (CH_2)	1445
ν (CO) + δ (COH)	1249	ν_s (COO^-)	1411
ν (CN)	1142	ω (CH_2)	1337
τ (CO)	1044	ω (NH_2) + ν (CN)	1134/1119
ν (CC) + ω (NH_2)	937	ν (CN)	1038
ω (NH_2) + ν (CC)	896	ρ (CH_2)	919
δ (OCO)	679	ν (CC)	895
		ρ (COO^-)	705

Key: ν_{as} = asymmetric stretching mode, ν_s = symmetric stretching mode, ν = stretching mode, δ = scissoring mode, ω = wagging mode, δ_s = symmetric deformation mode, ρ = rocking mode, τ = torsion.

3.3 Adsorption of glycine on non-crystalline ice

The influence of glycine on a NCI surface is demonstrated in Figure 3.6, which shows the development of the RAIRS spectra in early stage of glycine deposition. Particular attention has been paid to the region where NCI displays a weak feature at 3696 cm^{-1}, which is related to the dangling OH bond, shown as an inset in Figure 3.6, as the latter is generally used to monitor the effect of molecular adsorption on ice surfaces [26]. The glycine adsorption on the bare NCI surface at 119 K induces significant changes at the very beginning for the peak at 3696 cm^{-1}, which gradually decreases in intensity, indicating that there exists some interaction between the dangling OH bond and glycine molecules. It can be suggested that the species are bound to the NCI surface via hydrogen bonding. After 5 minutes exposure at 5.4 nTorr (1.71 L), the free OH peak is no longer visible, which suggests that the non-hydrogen-bonded sites are completely occupied by

adsorbed glycine molecules [25]. This situation can be defined as monolayer coverage of glycine. In the case of the broad OH stretching vibration band at 3394 cm^{-1}, its intensity increases initially and then decreases once the surface free OH becomes saturated. An explanation to this is that when glycine is adsorbed on an ice surface, the adsorbed species reduces the disorder of the ice surface, and reconstruction occurs within the surface [31]. That is why initially we observe a small increase in the OH stretching peak followed by a reduction in intensity. The decrease in the intensity of the OH stretching band suggests that the adsorbate begins to interact with the surface bilayer of the ice film, which can be confirmed by the appearance of a few peaks associated with the glycine molecule in the 1800-1250 cm^{-1} region, shown as an inset in Figure 3.6. The first few peaks that appear during the early stage of adsorption are 1712, 1652, 1442, 1418 and 1336 cm^{-1} and these are assigned as C=O stretching, NH_2 scissoring, CH_2 scissoring, COH scissoring and CO stretching and CH_2 wagging modes, respectively. It is clear from the appearance of these peaks that both the NH_2 and COOH functional groups are interacting with the ice surface. It should be noted that the librational mode at ~ 895 cm^{-1} for the ice film continues to increase, while the combination band at 2237 cm^{-1} remains unchanged with exposure.

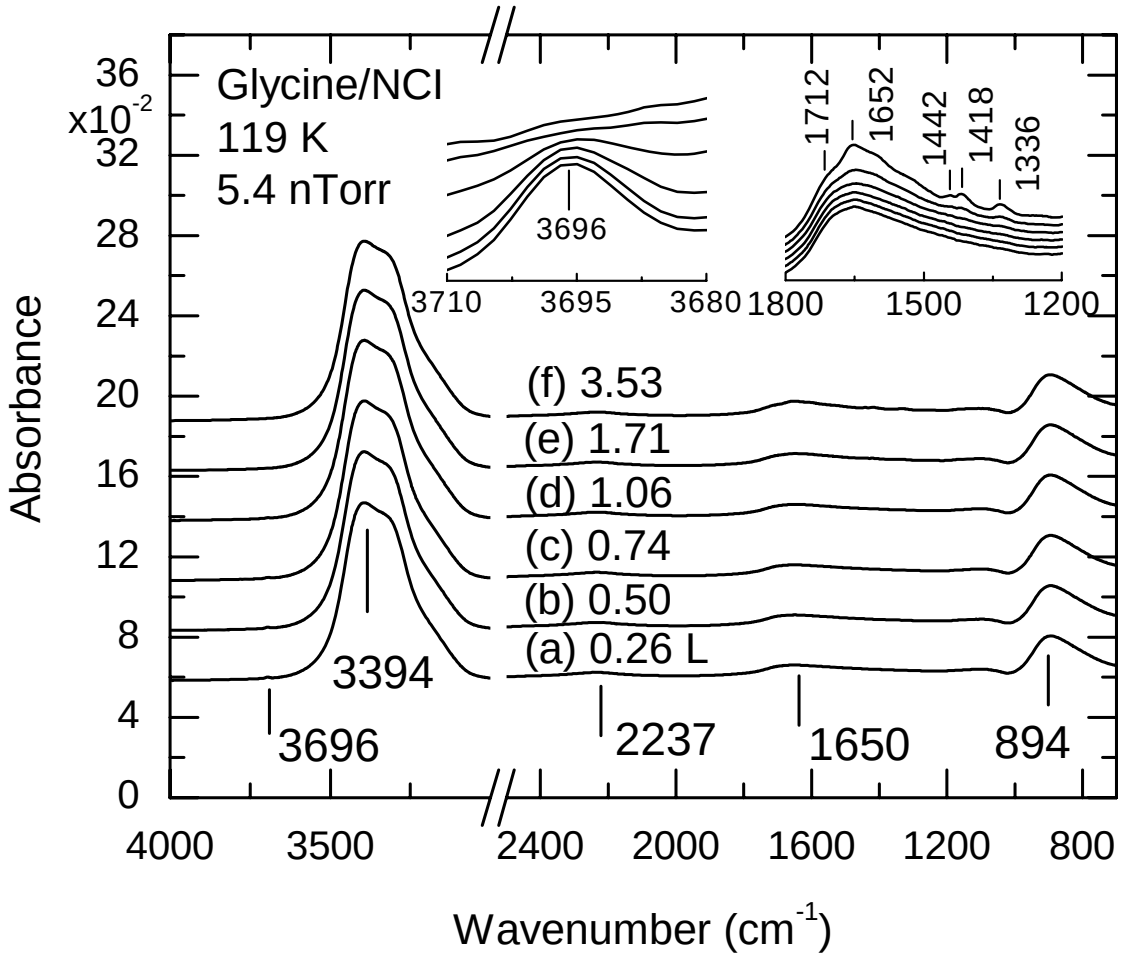

Figure 3.6: RAIRS spectra of (a) 0.26 L, (b) 0.50 L, (c) 0.74 L, (d) 1.06 L, (e) 1.71 L, and (f) 3.53 L of glycine deposited on NCI at 119 K.

Figure 3.7 displays the RAIRS spectra for further adsorption of glycine on non-crystalline ice. With increasing exposure, the RAIRS spectra evolve in a manner consistent with multilayer formation. The intensity of the OH stretching band decreases steadily and its peak position undergoes a small red-shift as further adsorption of glycine molecules occurs on the ice surface. This is correlated by the continuous growth of the bands in the 1900-700 cm^{-1} region [Figure 3.7(A)], in addition to a few peaks appearing in the 3100-1900 cm^{-1} region [Figure 3.7(B)]. For the 7.56 L exposure, the peak at 1660

cm^{-1} becomes more prominent and it was assigned to the NH_2 scissoring mode. Moreover, the features at 1418 and 1336 cm^{-1}, associated with the COH scissoring and CO stretching and the CH_2 wagging vibrations, respectively, are seen at that particular exposure. Another interesting feature that was previously observed for the glycine deposition on polycrystalline Cu at 121 K is the shoulder appearing at 1712 cm^{-1}, which corresponds to the C=O stretching vibration of the –COOH group, indicating that the glycine species adsorbed in its neutral form as found in the low-temperature experiment on the bare Cu. During the adsorption process, the combination band for the ice film at 2237 cm^{-1}, is seen to decrease for the 14.04 L exposure and a hump at 2099 cm^{-1} appears [Figure 3.7(B), Inset]. Coupled with the latter observation, we observe the appearance of a very weak but sharp peak at 2340 cm^{-1}, which becomes more prominent at 21.66 exposure [Figure 3.7 (B) (d)]. The latter peak may be an indication of multilayer formation for the low temperature experiments, as it was previously observed for adsorption of glycine on Cu at 121 K. At 21.66 L exposure, the infrared band shapes and positions of glycine-related modes for the adsorption of glycine on NCI are almost the same as those observed for glycine deposited on polycrystalline Cu at 121 K, which could suggest that the orientation of the glycine species is similar in both cases. In the high-wavenumber region [Figure 3.7(B)], the peaks are not as sharp as those observed for the glycine adsorption on polycrystalline Cu at low temperature (Figure 3.4). A plausible reason could be that they are masked by the strong broad OH stretching band, which is the dominating band, of the ice film.

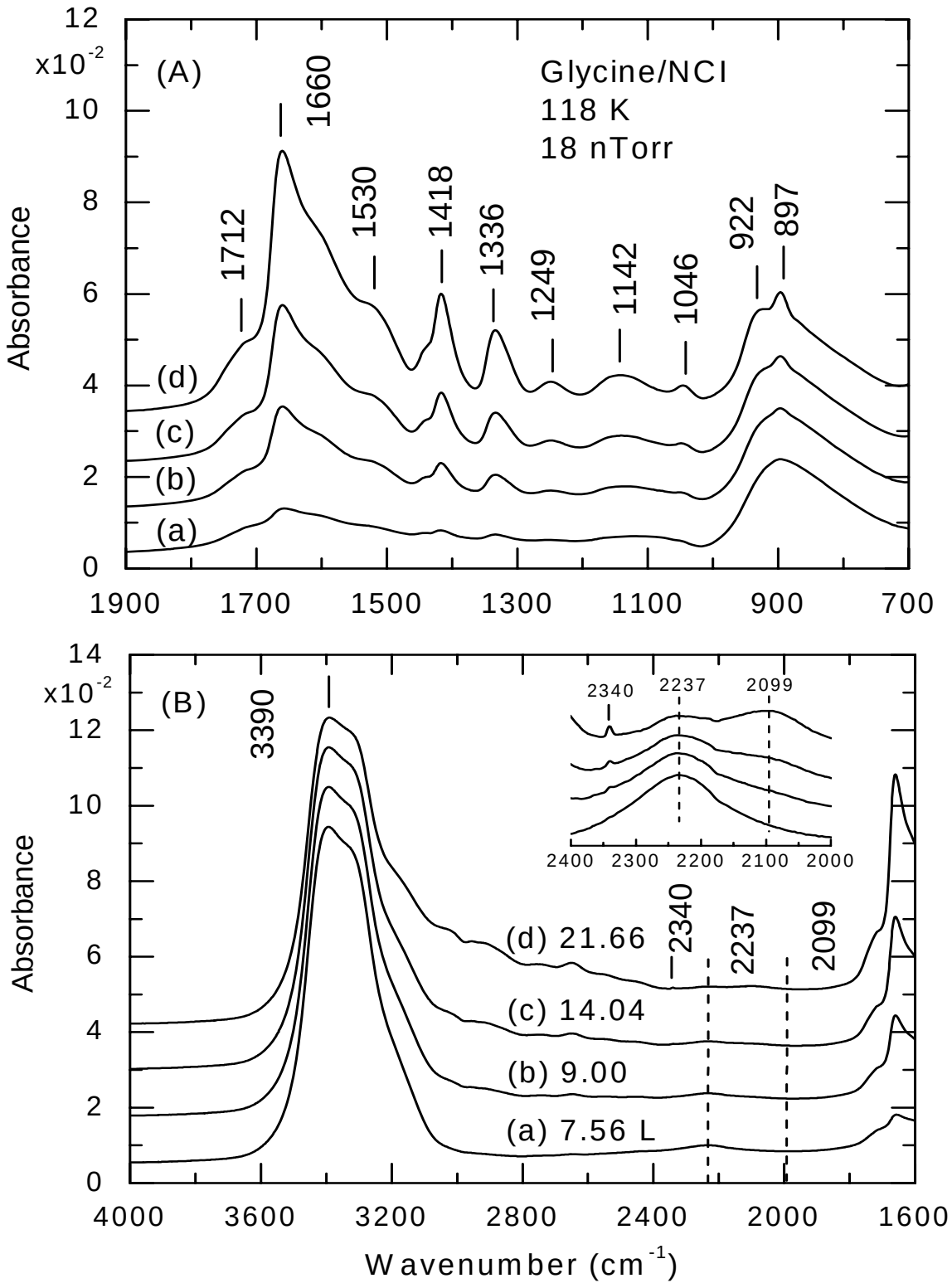

Figure 3.7: RAIRS spectra of (a) 7.56 L, (b) 9.00 L, (c) 14.04 L and (d) 21.66 L of glycine deposited on NCI at 118 K.

3.4 Thermal evolution of glycine adsorbed on non-crystalline ice

Following the maximum exposure of gaseous glycine species (20 minutes exposure) at 18 nTorr to the NCI surface, the sample was gradually annealed while acquiring data in order to study the thermal evolution of the adsorbed species on the NCI surface. In order to observe the effect of heat on the adsorbed species on NCI, a slow heating rate of 0.02 K/s was initially used and RAIRS spectra acquired simultaneously. Once the ice film has desorbed, a higher heating rate was used. Figure 3.8 shows selected spectra recorded during the sample annealing from 120 K with a heating rate of 0.02 K/s. Starting from 149 K to 159 K, the OH stretching band of NCI located at 3390 cm^{-1}gradually decreases in intensity [Figure 3.8(B)]. This observation is described as the onset of crystallization of ice and is accompanied by an increase in intensity of the NH_2 scissoring mode at 1660 cm^{-1}. The observed asymmetric peak profile of the OH stretching band is associated with the non-crystalline to polycrystalline phase transition [30]. This phenomenon is due to the collapse of the NCI pores during the evolution towards the PCI. On the other hand, the disappearance of the C=O stretching vibration of the –COOH group at 1712 cm^{-1} indicates that the neutral acidic group is being converted to the COO^- species, suggesting that the proton is lost from the adsorbed species. However, it is not clear at this stage whether the proton is lost as H_3O^+ or rather transfers to the NH_2 group. In addition, the observed decrease in the intensity of the peak around 1249 cm^{-1}, corresponding to the CO stretching and COH scissoring modes, is consistent with the proton transfer from the carboxyl group to the amino group of the adsorbed species on the NCI. This observation can actually be used to explain the rise in the NH_2 scissoring mode. Because the COO^- stretching vibration occurs in the same wavenumber range, it may be possible that this

mode is masked by the NH_2 scissoring mode, which increases in intensity as the band at 1712 cm^{-1} weakens. After annealing up to 164 K, the red-shift of OH stretching vibration from 3390 cm^{-1} to 3292 cm^{-1} is considered as a transition from non-crystalline ice phase to a polycrystalline ice phase with a decrease of the local disorder of the ice structure and an increase in the intermolecular coupling of water molecules in the ice film [Figure 3.8 (B)]. Another interesting feature is seen at 1530 cm^{-1}, which appears as a shoulder at 120 K, but becomes better defined at 164 K. From the previous section, a peak appearing at 1534 cm^{-1} was assigned to NH_3^+ symmetric deformation. The value that we observe closely matches the literature [36] and we may therefore suggest a proton transfer from the –COOH group to the $–NH_2$ group. Moreover, the very weak but sharp peak at 2341 cm^{-1} [Figure 3.8(B), Inset] shows a decrease in intensity with increasing annealing temperature. Between 120 K and 164 K, the intensities of the remaining bands remain essentially unchanged, which is indicative of a stable adsorption state of the glycine species. For annealing in the temperature range of 149–164 K, two major observations were made. Firstly, thermal destabilization of the ice occurs in that temperature range and secondly the proton transfer phenomenon in the glycine adspecies was observed. Based on the features that are characteristic of the glycine species, we can also conclude that no desorption of any glycine adspecies has yet taken place in this temperature range.

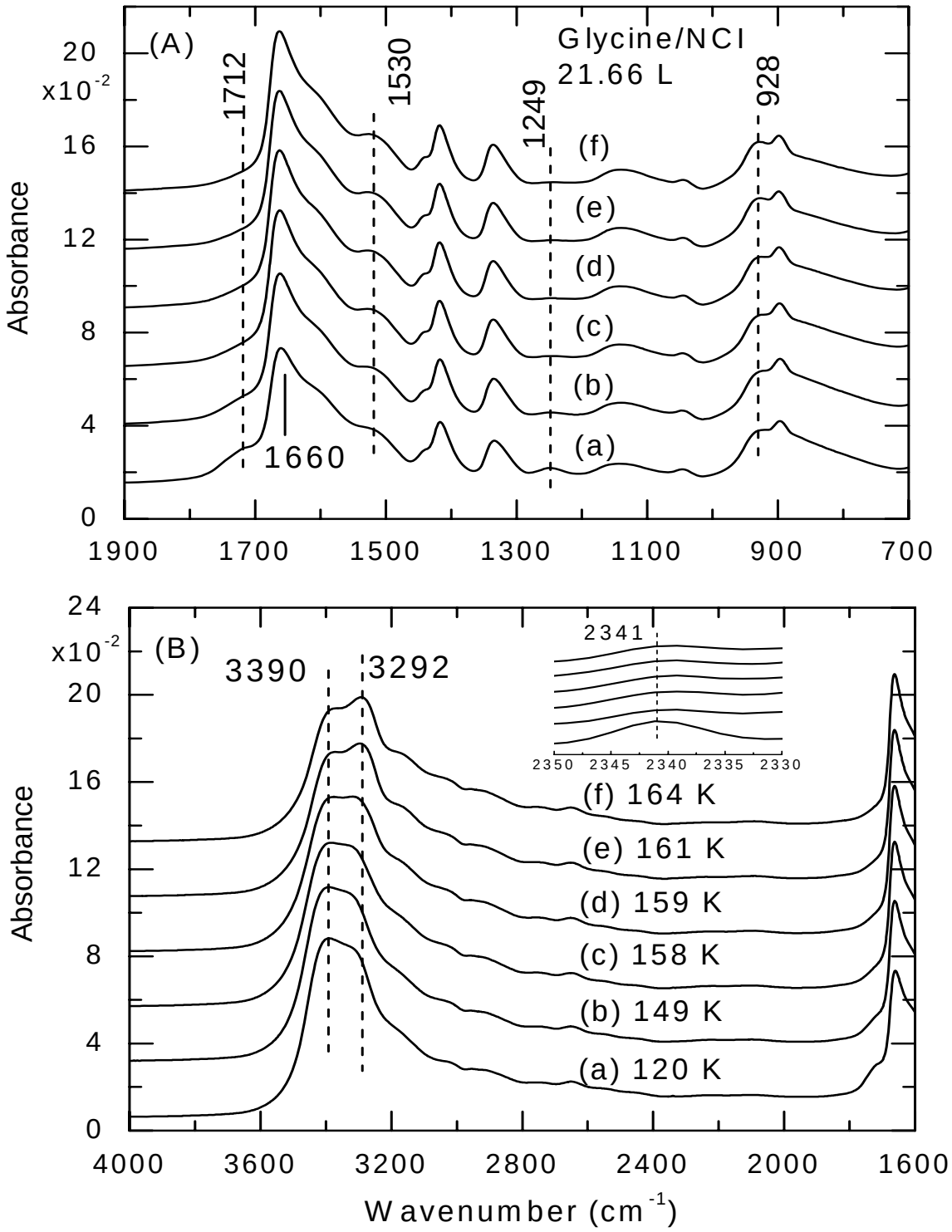

Figure 3.8: RAIRS spectra of 21.66 L of glycine deposited at 18 nTorr on a NCI film at 118 K as a function of annealing temperature: (a) 120 K, (b) 149 K, (c) 158 K, (d) 158 K, (e) 161 K, and (f) 164 K.

Further annealing the sample to 292 K produces no major changes in the RAIRS spectra in the low-wavenumber region, shown in Figure 3.9 (A). Considering the high-wavenumber region at 292 K, the OH stretching band of the ice film at 3292 cm^{-1} has been totally eliminated. The absence of the latter peak implies that the ice film has completely desorbed from the Cu support. Moreover, a gradual decrease in the intensity of the peak at 1660 cm^{-1} can be seen from 173 K to 292 K. However, important modifications are observed in the infrared bands at 302 K. In particular, Figure 3.9 (B) (e) indicates an abrupt growth of a peak at 3185 cm^{-1}. The latter is in accordance with the observed NH_3^+ asymmetric stretching band at 3187 cm^{-1} for the glycine deposition on the Cu sample at room temperature. Most remarkably in the low-wavenumebr region [Figure 3.9 (A)] is the sudden red-shift of the peak at 1660 cm^{-1} to 1648 cm^{-1} along with an enhancement in intensity of the peak at 1648 cm^{-1}, when the sample was annealed at 302 K. A plausible explanation is that complete transformation of the neutral glycine to its zwitterionic form occurs at 302 K. At 302 K, the CC stretching and NH_2 wagging modes at 929 and 898 cm^{-1} shift to 925 and 889 cm^{-1}, respectively. Interestingly, the relative intensity distribution between the two features switches. At 164 K, the lower wavenumber band is the more intense whereas at 302 K, this is the one of lower intensity. It is also informative to note the enhancement of the peak at 1520 cm^{-1} which previously occurred as a shoulder. The latter band is assigned to the NH_3^+ symmetric deformation mode. On the basis of the observation, the following scenario may be suggested. Neutral adsorbed glycine on the NCI film is converted to its zwitterionic form upon warming the substrate. Once complete desorption of the ice film from the Cu surface occurs, the glycine species undergo reorientation and settle on the Cu surface.

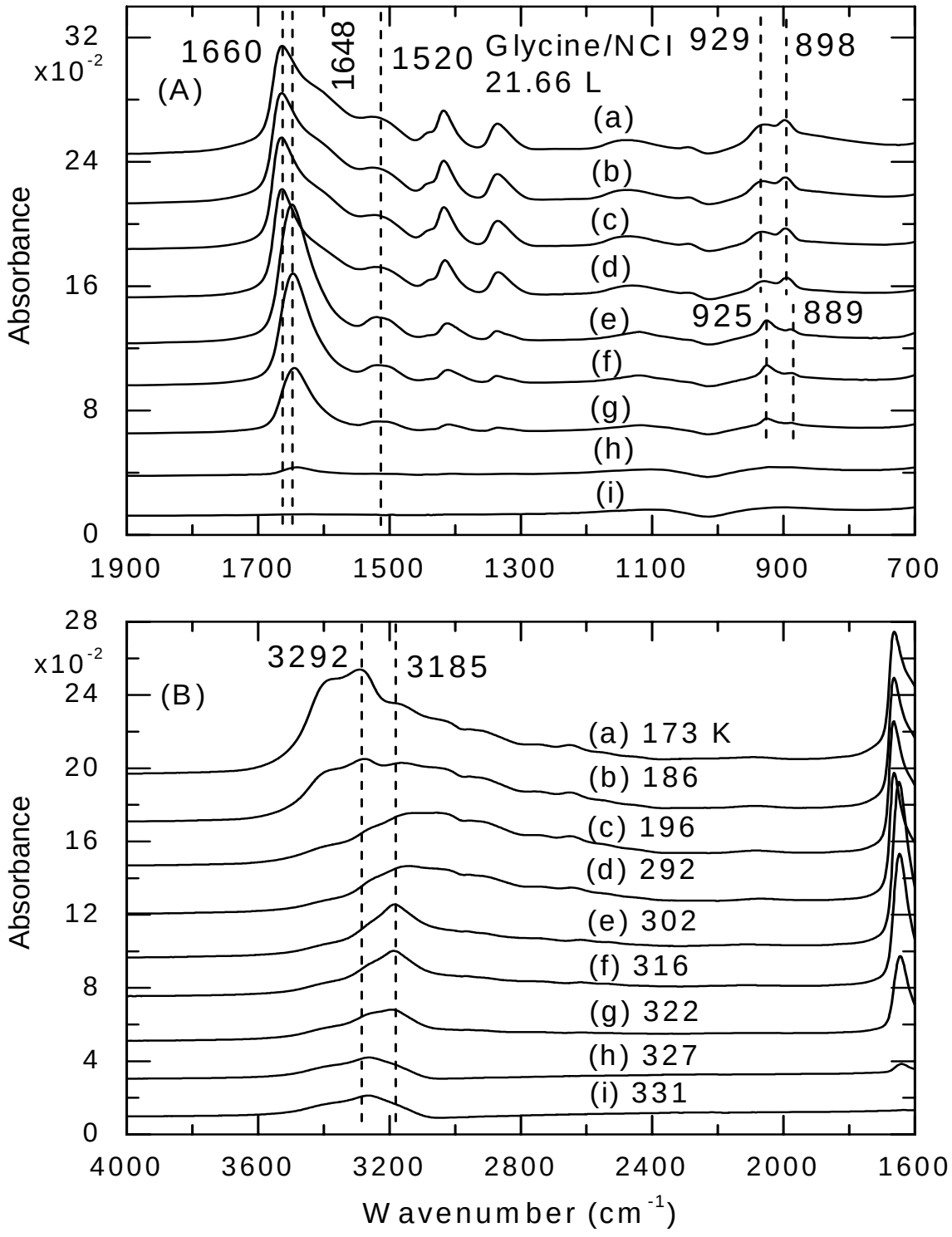

Figure 3.9: RAIRS spectra of 21.66 L of glycine deposited at 18 nTorr on a NCI film at 118 K as a function of annealing temperature: (a) 173K, (b) 186 K, (c) 196 K, (d) 292 K, (e) 302 K, (f) 316 K (g) 322 K, (h) 327 K and (i) 331 K.

3.5 Adsorption of glycine on polycrystalline ice

The adsorption of glycine on a polycrystalline ice film was conducted with the substrate held at 160 K. The RAIRS spectra associated with the low exposure phases are plotted in Figure 3.10. Exposure of glycine to the ice surface at this level results in strong hydrogen bonding of the glycine species to the OH dangling bond site. In particular, the free OH of the ice surface at 3694 cm^{-1} decreases gradually in intensity until complete extinction as glycine is adsorbed on the surface [Figure 3.10 (B), Inset]. The disappearance of the 3694 cm^{-1} peak is an indication that surface adsorption of the glycine species and the ice film top layer surface has ended. Another important modification in the ice spectrum is observed in the position and intensity of the bulk OH stretching feature at 3247 cm^{-1}. The latter is shifted to lower wavenumber by 6 cm^{-1}. This red-shift can be explained in terms of the strengthening of the hydrogen bond network in the ice structure [14]. The shift in wavenumber occurs in conjunction with some major glycine features, namely at 1660, 1442, 1416 and 1334 cm^{-1} in the low-wavenumber region. These peaks are assigned to the NH_2 scissoring, CH_2 scissoring, COH scissoring and CO stretching and CH_2 wagging modes, respectively. The appearance of these major peaks at 1.80 L exposure [Figure 3.10 (A) (e)] can be associated with a particular adsorption geometry of the glycine adspecies on the PCI film. At 2.16 L exposure, the peak at 898 cm^{-1}, corresponding to NH_2 wagging and CC stretching modes, start to grow. The distinct band attributed to NH_2 scissoring mode indicates hydrogen bonding interaction between the surface bilayer and the amino group. Moreover, the emergence of the bands at 1416 and 1334 cm^{-1} which are clearly seen at 1.80 L exposure, shows that the carboxyl group is also interacting with the ice film, most probably via strong hydrogen bonding. This is confirmed by the shoulder

occurring at 1720 cm^{-1}. The latter C=O stretching vibration indicates that the adsorbed species contains the –COOH acid group. However, it is not clear whether the adsorbed glycine has the NH_2 or NH_3^+ group because in addition to the NH_2 scissoring mode at 1660 cm^{-1}, a shoulder at 1531 cm^{-1} can also be observed, which was previously assigned to the NH_3^+ deformation mode.

The RAIRS spectra of glycine deposited on polycrystalline ice films at higher glycine exposure are shown in Figure 3.11. Evidently, a number of changes occur at higher glycine exposure. The position as well as the intensity of the broad OH coupled band [Figure 3.11 (B)] changes, with the peak position changing from 3239 cm^{-1} for a 7.14 L exposure to 3231 cm^{-1} for a 11.22 L exposure. This can be interpreted as the reconstruction of the ice structure as foreign molecules are embedded in the ice film such that the micropores collapse upon further glycine adsorption [14]. In parallel with the decrease in intensity of the OH stretching mode, another notable difference occurs for the scissoring mode band. The hump appearing at 2237 cm^{-1}, related to the ice film, is seen to lower gradually in intensity with glycine exposure from 7.14 L exposure to 11.22 L exposure, and ultimately giving rise to another shoulder at 2093 cm^{-1}. The latter is clearly seen at 11.22 L exposure. This effect can presumably be attributed to intermolecular interactions of the glycine adspecies and the near surface ice film. In conjunction with the changes occuring in the high-wavenumber region, the relative intensity of the peaks in the 1900–700 cm^{-1} region show remarkable increase. It appears that a new feature at 933 cm^{-1}, which is attributed to the CC stretching and NH_2 wagging modes, begin to grow at 8.16 L exposure. Since we are able to see the CC stretching and NH_2 wagging modes at 8.16 L exposure, there must be a significant component of the dipole moment associated

with this vibration that is perpendicular to the surface. In addition to these features, additional peaks are seen at 1143 and 1044 cm^{-1} for the 8.16 L exposure. They are assigned to CN stretching vibration. Moreover, the hump growing at 1250 cm^{-1}, which becomes evident at 10.20 L exposure, corresponds to the CO stretching and COH scissoring modes. This suggests the possibility of a different orientation of the glycine molecule at that higher exposure. The continuous growth of the glycine related peaks at 11.22 L exposure, with no major changes in the shape of the peaks, suggests multilayer formation. Compared to the adsorption of glycine on NCI, there is no major difference in the peak positions from those of the RAIRS spectra for glycine adsorbed on PCI, with the exception of the C=O stretching band being less prominent in the case of PCI. In addition, the peak at 1525 cm^{-1} is more evident in the case of adsorption of glycine on PCI, whereas it is seen as a shoulder in the case of glycine adsorption on NCI.

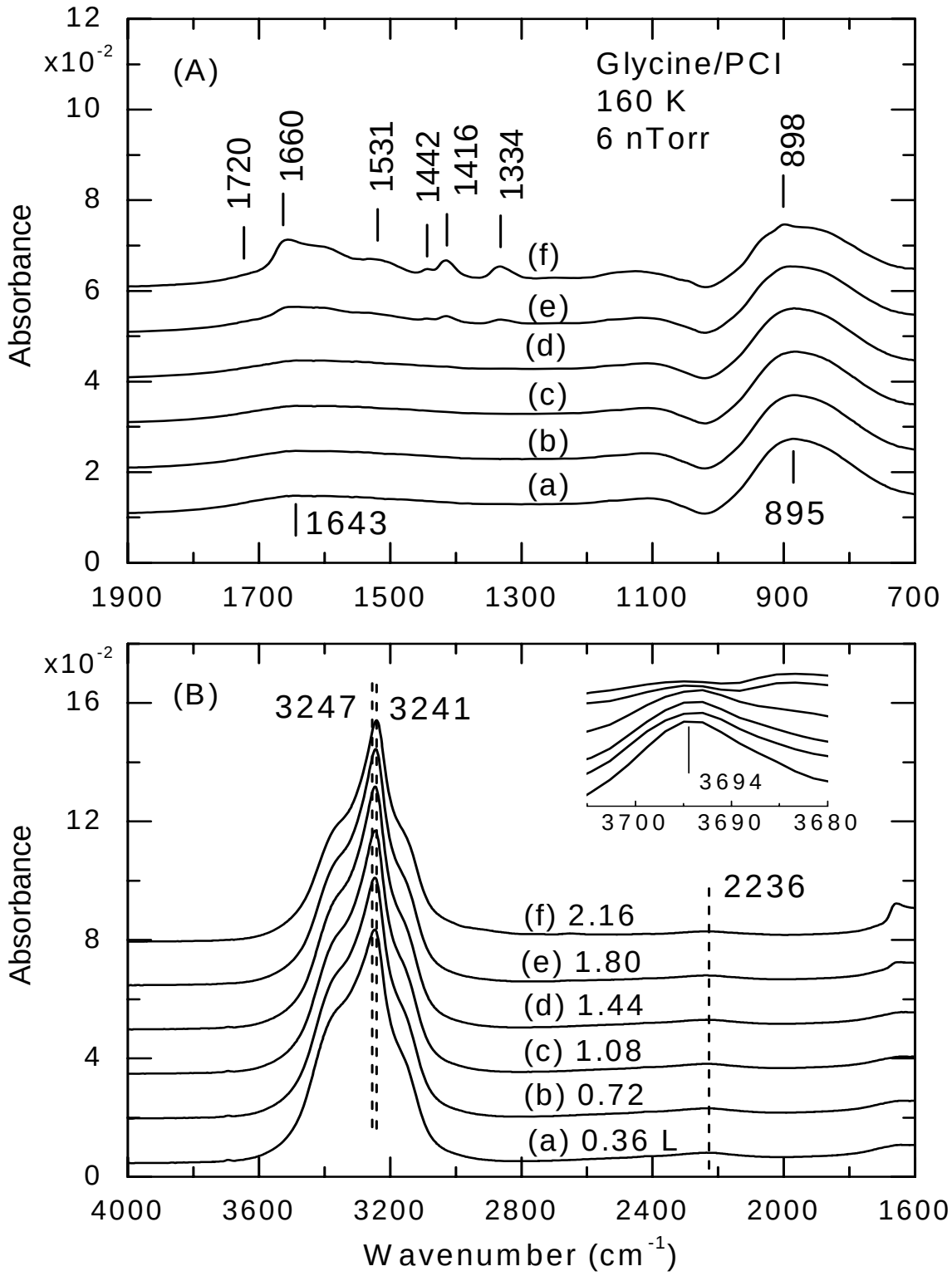

Figure 3.10: RAIRS spectra of (a) 0.36 L, (b) 0.72 L, (c) 1.08 L, (d) 1.44 L, (e) 1.80 L and (f) 2.16 L of glycine deposited on PCI at 160 K.

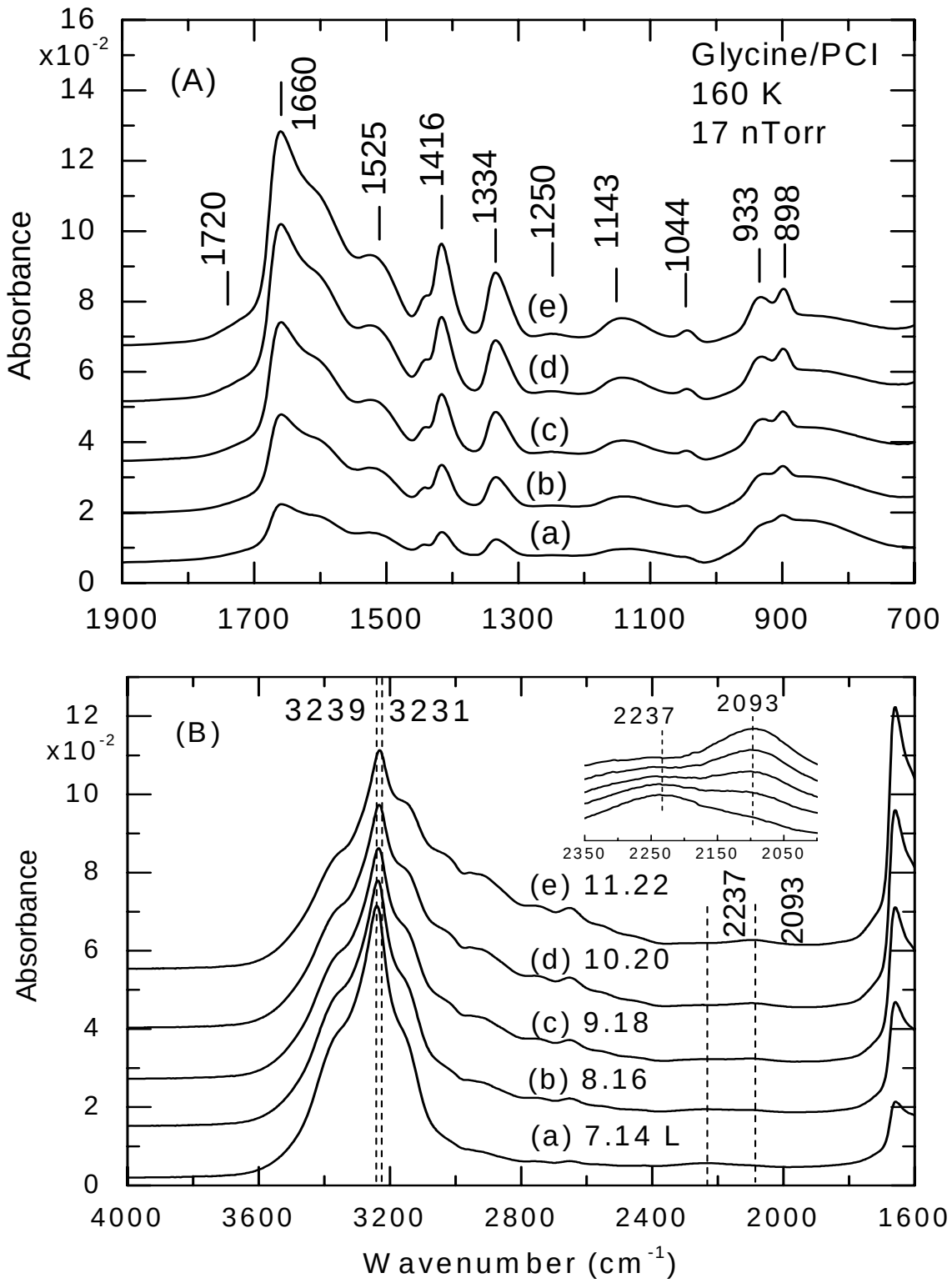

Figure 3.11: RAIRS spectra of (a) 7.14 L, (b) 8.16 L, (c) 9.18 L, (d) 10.20 L and (e) 11.22 L of glycine deposited on PCI at 160 K.

3.6 Thermal evolution of adsorbed glycine on polycrystalline ice

Figure 3.12 shows a series of RAIRS spectra for the thermal evolution of glycine bound to PCI film produced at various annealing temperatures. Major changes occur in the high-wavenumber region for low annealing temperatures, and the infrared bands for the 4000–1600 cm^{-1} spectral range are presented in Figure 3.12 (B). Figure 3.12 (A) shows the changes occurring in the 1900–700 cm^{-1} region. The influence of annealing on the adsorbed species on PCI is demonstrated by a decrease in intensity of the OH stretching band at 3231 cm^{-1} at 151 K. This may be attributed to a loss of ordered arrangement of the hydrogen-bonded network as the substrate is annealed at an initial rate of 0.035 K/s. As heat is provided to the substrate causes the bonds within the ice structure to become soft. Further annealing to 236 K results in complete desorption of the ice film from the Cu support, as evidenced by the disappearance of the OH stretching band at 3231 cm^{-1}. Moreover, when the substrate is annealed to 236 K, the hump at 2101 cm^{-1} is shifted to 2081 cm^{-1}. No significant changes in the peaks associated with the glycine adspecies in the high-wavenumber region are observed. However, an important phenomenon takes place in the low-wavenumber region, which is marked by the disappearance of the shoulder appearing at 1720 cm^{-1} along with the feature at 1250 cm^{-1} at 236 K. The latter band is associated to the CO stretching and COH scissoring modes, while the former is assigned to the C=O stretching vibration. The disappearance of the band at 1720 cm^{-1} implies the loss of the proton from the acid carboxyl group. Consequently, the proton is transferred to the amino group, indicated by the enhancement of the NH_3^+ deformation mode at 1525 cm^{-1}. In addition, the CN stretching mode at 1044 cm^{-1} broadens with increasing annealing temperature. We can therefore suggest that reorientation of the

glycine species is taking place. On the other hand, the most prominent band at 1660 cm^{-1} increases in intensity. These observations are consistent with the results obtained for the case of the thermal evolution of glycine on NCI, whereby the proton from the COOH group being transferred to the NH_2 group upon annealing. An explanation to this is that a liquid-like surface is produced upon annealing of a thin ice film [17] and therefore the glycine molecule has an opportunity to solvation. In an aqueous environment, the zwitterionic form of glycine predominates. Just as for the case of thermal evolution of glycine on NCI, once the ice film desorbs completely from the Cu support, the glycine species bind to the Cu surface.

Figure 3.13 shows additional RAIRS spectra collected at higher (268–325 K) temperature range. A comparison of the spectrum at 268 K from that at 236 K shows no significant changes in the absorption bands. However, considerable spectral changes were observed after annealing the sample to 298 K. The NH_2 scissoring mode at 1660 cm^{-1} undergoes a red-shift accompanied by a sudden rise in intensity. The peak position is now centered at 1643 cm^{-1}, and could be attributed to the COO^- asymmetric stretching vibration. Moreover, the enhancement in intensity of the band at 1525 cm^{-1} after annealing to 298 K indicates that a different orientation of the adsorbed species might exist on the surface. The latter band has previously been assigned to NH_3^+ deformation mode. Moreover, the feature at 1143 cm^{-1} undergoes a red-shift to 1121 cm^{-1}. As it can be observed, the shape and intensity of the CC stretching and NH_2 wagging absorption bands, respectively, at 930 and 895 cm^{-1} are reversed at 298 K, with the former peak dominating over the other one. It should also be noted that both peaks undergo a 5 cm^{-1} red-shift. This observation is similar to that made earlier for the thermal evolution of

glycine on NCI. In addition, the high-wavenumber region [Figure 3.13 (B)] is marked by the appearance of a sharp peak at 3175 cm^{-1} for the 298 K anneal. This peak has been previously observed for glycine adsorption on polycrystalline Cu at room temperature, but is absent in the low-temperature experiment. It was assigned to the NH_3^+ asymmetric stretching vibration. Moreover, the feature located at 2106 cm^{-1} is shifted to lower wavenumber (2073 cm^{-1}) and is of lower intensity. The disappearance of the band at 3042 cm^{-1} with increasing annealing temperature, suggests loss of intermolecular hydrogen bonding interaction between the glycine molecules in the multilayer. This indicates that no multilayer exists at 298 K. With further annealing, from 298 to 325 K, the band shape is rather unchanged, but the intensities of the glycine related bands decrease with increasing temperature. These observations demonstrate that once the ice desorbed from the surface, the glycine species bind to the Cu surface as a zwitterionic species. At 320 K, the glycine species desorbs from the Cu surface.

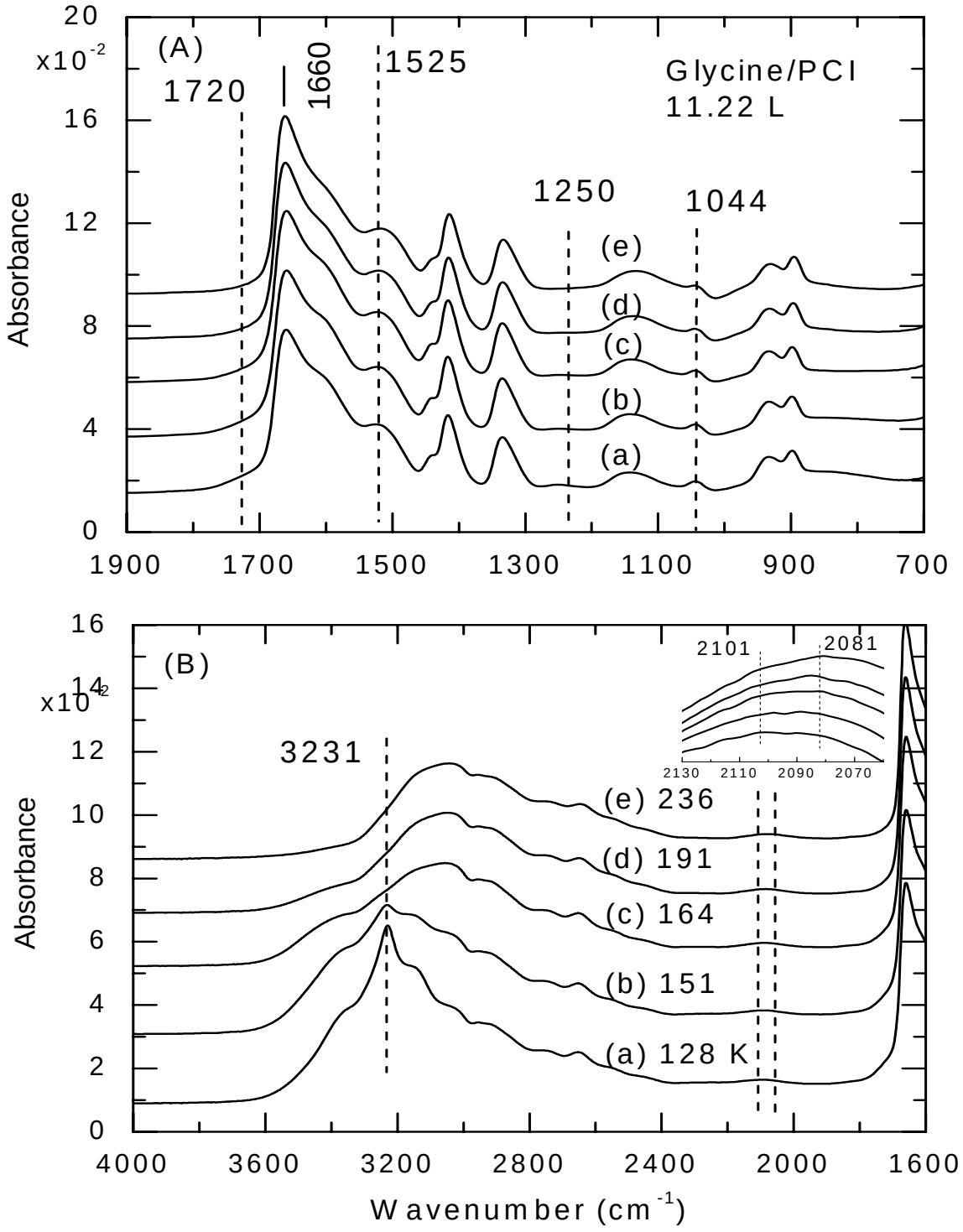

Figure 3.12: RAIRS spectra of glycine deposited at 17 nTorr on a PCI film at 160 K as a function of annealing temperature: (a) 128 K, (b) 151 K, (c) 164 K, (d) 191 K and (e) 236 K.

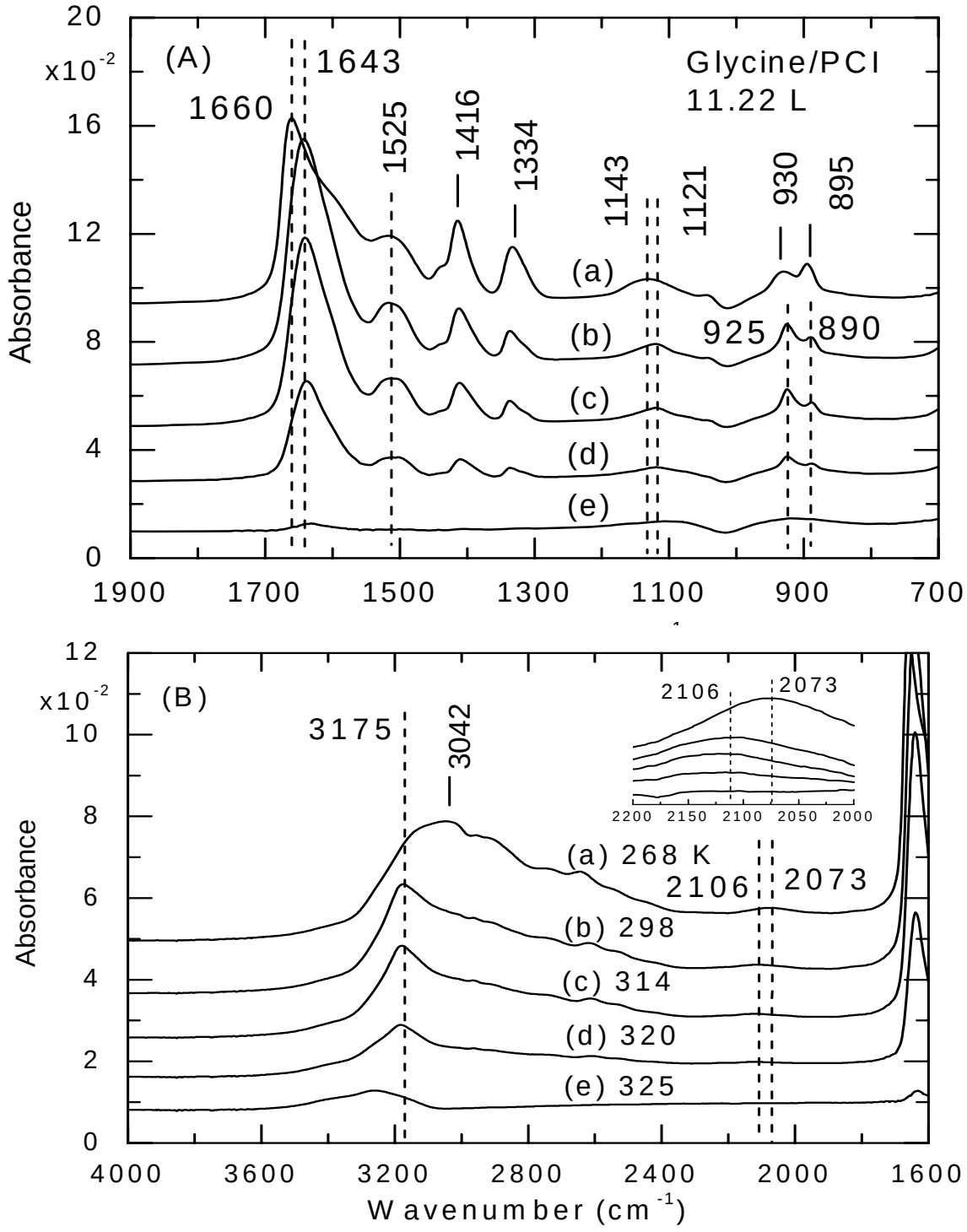

Figure 3.13: RAIRS spectra of glycine deposited at 17 nTorr on a PCI film at 160 K as a function of annealing temperature: (a) 268 K, (b) 298 K, (c) 314 K, (d) 320 K and (e) 325 K.

As a first approach to the study of the interaction of organic molecules with surfaces, we have successfully investigated the adsorption of glycine, the simplest amino acid, on different surfaces, including polycrystalline Cu, NCI and PCI surfaces by utilising reflection-absorption infrared spectroscopy. It has been shown that the interaction of organic molecules with different surfaces greatly depends largely on the exposure and thermodynamic conditions, such that the molecular orientation at low exposure differs from that at high exposure. Moreover, room-temperature experiment revealed a different adsorbed species as compared to low-temperature experiments, as illustrated by the RAIRS spectra. An extension of the present study is to tackle the next amino acid, alanine. In particular, alanine exists in two different enantiomeric forms, the L and D alanine. Due to the fact that chirality is observed in alanine, it would be of great interest to gain an understanding on how this organic chiral molecule binds to the aforementioned surfaces employed earlier for the study of glycine. So the next step is to investigate the interaction of both L and D alanine species on polycrystalline Cu, NCI and PCI surface by RAIRS.

3.7 Adsorption of L-alanine on polycrystalline Cu at two different temperatures

Films of L-alanine were deposited on the polycrystalline Cu surface held at 123 K by evaporation of the alanine powder contained in a crucible inside the high-flux beam doser. Figure 3.14 shows the RAIRS spectra of L-alanine at the very beginning of exposure. The adsorption behaviour of L-alanine on polycrystalline Cu at low exposure reveals that the molecule exists in its neutral form, as was similarly observed for the

glycine adsorption. This is clearly indicated by the appearance of the C=O stretching band due to the intact –COOH acid group at 1711 cm^{-1} at 0.18 L coverage [Figure 3.14 (A) (a)]. It is therefore proposed that there exists an interaction between the carboxyl group and the Cu surface at that particular coverage. In addition, there is an intense band growing at 1597 cm^{-1}, attributed to the NH_2 scissoring mode [49, 50, 51, 52], which implies that the amino acid is bound to the surface via the nitrogen atom of the NH_2 group. We also note the sharp peak at 1405 cm^{-1}, which is reported as the CH_3 symmetric scissoring mode [44, 53]. While these bands continue to evolve at 1.44 L exposure, with the peaks at 1723 and 1711cm^{-1} still growing as a doublet, new features are observed at 1465, 1371, 1352, and 1305 cm^{-1} and can be attributed to CH_3 asymmetric scissoring [44,50–53], CH_3 symmetric scissoring [44, 51, 52], CH scissoring [51, 52], and CH deformation [44, 49, 50, 53] modes respectively. Three additional peaks are also observed at 2990, 2946 and 2897 cm^{-1} in the high-wavenumber region at 1.44 L exposure [Figure 3.14 (B)]. The latter peaks are assigned to NH_3^+ symmetric stretching [53] or CH_3 asymmetric stretching [44], CH_3 asymmetric stretching [51–53] or CH_3 asymmetric stretching [44], and CH stretching [50–52] or CH_3 scissoring [44] vibrations, respectively.

The RAIRS spectra of L-alanine obtained at higher exposure are shown in Figure 3.15. At 9.60 L, an increase in intensity of the previously described bands for the 1.44 L exposure is observed. It is interesting to note the behaviour of the C=O stretching band at 1711 cm^{-1} at higher exposure. The latter band is higher in intensity than the peak at1723 cm^{-1}. In contrast, the NH_2 scissoring mode at 1649 cm^{-1} is seen to dominate over the peak found at 1612 cm^{-1}. This is clear evidence that the adspecies undergo molecular

rearrangement. The spectrum for the 13.20 L exposure exhibits additional peaks mainly in the fingerprint region. In particular, the RAIRS spectrum is dominated by the the NH_2 scissoring mode, at 1649 cm^{-1}, and other weaker features at 1465, 1411, 1371, 1352. 1305, 1226, 1119, 917, 845 and 773 cm^{-1} are observed. The 16.92 L exposure is comparable to the 13.20 L exposure when considering the low-wavenumber region, with an additional peak at 823 cm^{-1} in addition to a hump appearing at 1010 cm^{-1}. At 16.92 L exposure, the adsorption peaks become more distinct in the high-wavenumber region, especially for the hump at 2109 cm^{-1}. This behaviour is strongly indicative of intermolecular hydrogen bonding occurring among adjacent L-alanine molecules in the multilayer phase. The 16.92 L exposure is also marked by the sudden increase of the peak intensities, and this is an indication of multilayer formation, evidenced also by the band appearing near 3000 cm^{-1}. The general features of the 21.00 L coverage are reproducible from the 16.92 L spectrum, with the exception of some variations in the relative intensities of the bands, justifying the multilayer formation. It should be noted that at 21.00 L exposure, the weak peak at 2897 cm^{-1}, which was observed at low exposure, is missing. The assignments for the main absorption peaks observed for the highest exposure are tabulated in Table 3.2.

The adsorption of L-alanine on polycrystalline Cu at 298 K yields a number of RAIRS spectra shown in Figure 3.16. The most interesting aspect of the RAIRS spectra obtained for L-alanine adsorbed on the polycrystalline Cu surface at room temperature is that they show variations with coverage, particularly with respect to the relative intensities and shapes of the absorption peaks. This behaviour suggests that a number of adsorption phases are formed under different conditions. Starting from the bottom, the

first two spectra [Figure 3.16 (a) and (b)] may be identified as low-coverage phase on the basis of the following explanation. Analysis of the RAIRS spectra show that the feature at 1711 cm^{-1}, characteristic of the carbonyl stretching vibration, is missing, suggesting that the L-alanine adspecies has an ionic character rather than the neutral form. During the early stage of exposure, the appearance of fewer bands at 1627, 1461, 1405 and 1373 cm^{-1}, attributed to COO^- asymmetric stretching, CH_3 asymmetric scissoring, COO^- symmetric stretching and CH_3 symmetric scissoring vibrations, respectively, is direct evidence of the deprotonation of the carboxylic acid group. The spectrum obtained after 20-minute exposure at 1200 nTorr or 1440 L [Figure 3.16 (b)] is nearly identical to the 540 L exposure, and is therefore attributed to the low coverage phase. This would imply that the terminal COO^- group of the L-alanine species is involved in bonding to the metal surface evidenced by the peak at 1627 cm^{-1}, assigned to COO^- asymmetric stretching. This suggests that there must be a dipole moment associated with this vibration that is perpendicular to the surface. It is important to note that at this particular coverage, the band at 1627 cm^{-1} dominates the one at 1405 cm^{-1}. Interestingly, there is some evidence that the species undergo structural changes upon further adsorption. The spectra for the 540 and 1440 L are dominated by the 1627 cm^{-1} band. Considering the 1800 L exposure [Figure 3.16 (c)], its profile reflects a change in the orientation of the species upon adsorption. This phase can be referred to as the intermediate coverage phase, and is marked by the appearance of new peaks both in the high and low-wavenumber regions. Further justification for this interpretation is provided by the behaviour of the bands in the 1700–1375 cm^{-1} region, where the sudden growth of the sharp peak at 1410 cm^{-1} is observed. Moreover, the band at 1627 cm^{-1} split into two corresponding components,

namely at 1637 and 1607 cm^{-1}. It should be noted that at this particular exposure, the convoluted peaks in the 1650–1580 cm^{-1} region are almost of the same intensity as compared to the sharp peak at 1410 cm^{-1}. Moreover, the 1800 L exposure is marked by the appearance of a few new weak features in the high-wavenumber region. These peaks are centered at 2941 and 2885 cm^{-1}, and are assigned to CH_3 asymmetric stretching and CH_3 scissoring modes, respectively [44]. This intermediate coverage phase may be considered as a transition into the high coverage phase and can therefore be attributed to monolayer coverage. Finally, the hig-coverage phase observed with further exposure (after 30 minutes) at 1200 nTorr [Figure 3.16 (e)] at room temperature is marked by possible changes in the bonding interaction. The spectrum is dominated by a strong sharp peak at 1410 cm^{-1}, assigned to the COO^- symmetric stretching mode. The variations in intensities and shapes of the features at 1637 and 1607 cm^{-1} indicate that the functional groups associated with these spectral features are changing in orientation with respect to the surface, with the peaks at 1637 being of lower intensity as compared to the peak at 1607 cm^{-1}. The high-wavenumber features at 2941 and 2885 cm^{-1} are seen to increase in intensity at higher exposure. It should be noted that at 298 K deposition temperature, the peak at 2941 cm^{-1} is the most intense peak while at low temperature, the peak at 2983 cm^{-1} dominated. We also reported the shoulder appearing at 1583 cm^{-1}, which is attributed to NH_2 scissoring mode [44]. The observed band wavenumbers, a total of 16, and their assignments for the L-alanine adsorption on polycrystalline Cu are listed in Table 3.2. From these observations, we can conclude that L-alanine adsorbs with the –COOH group on the Cu surface at low temperature, whereas at room temperature, the deprotonated species predominates. It should be pointed out that it is difficult to distinguish between

the wavenumbers associated with the NH_2 and NH_3^+ groups because they appear to be rather similar [36]. It is important to note that our data do not match completely with the earlier work reported by Williams et al. [44]. Williams et al. reported that the RAIRS spectra is dominated by the band at 1630 cm^{-1} for the high coverage phase, while in the present study, the band at 1410 cm^{-1} is of higher intensity as compared to the band at 1637 cm^{-1} at higher exposure. Moreover, in the present work, we observed splitting of the peaks at higher exposure. This situation has not been observed in Williams et al. work.

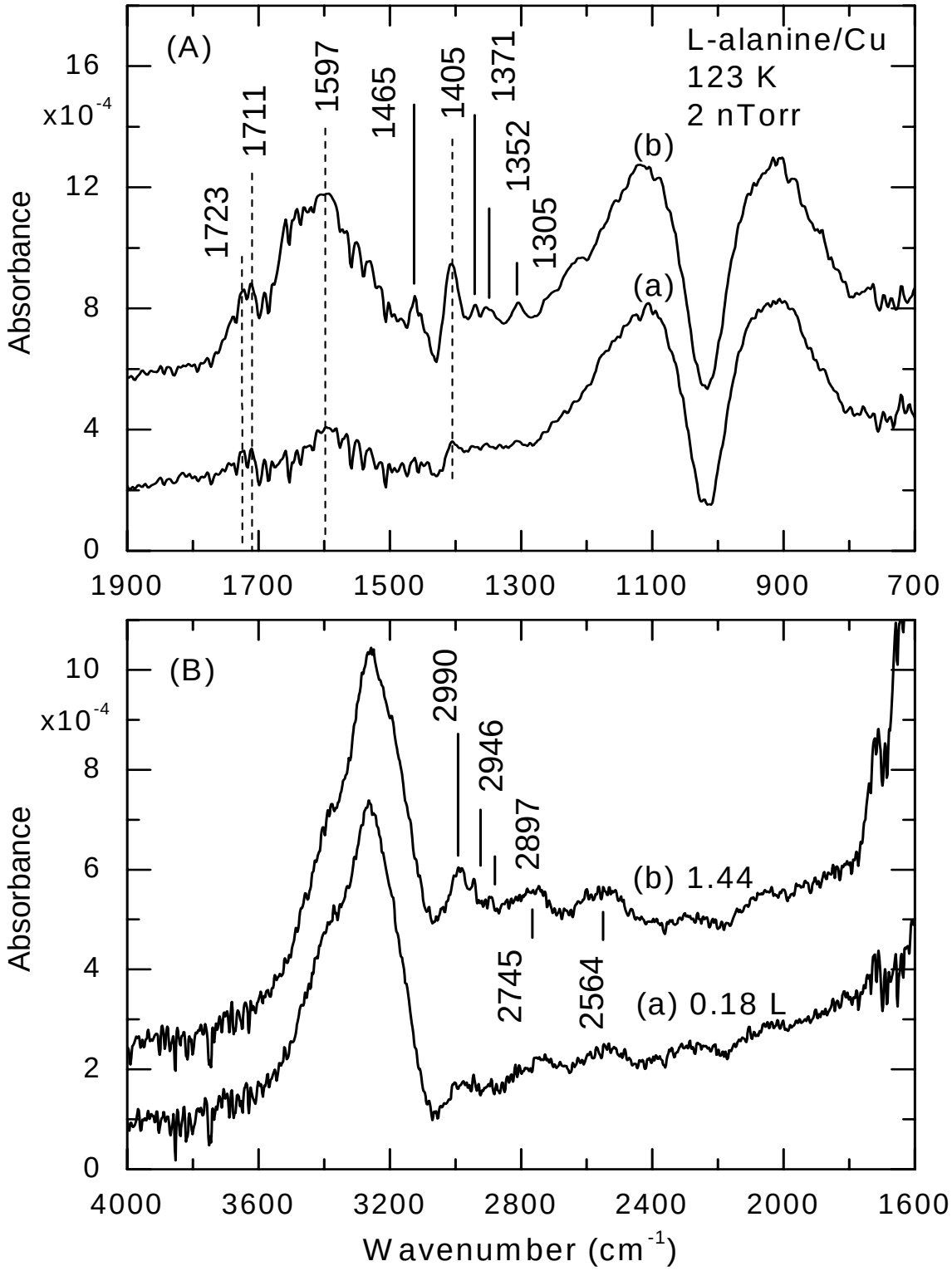

Figure 3.14: RAIRS spectra of (a) 0.18 L and (b) 1.44 L of L-alanine deposited on polycrystalline Cu at 123 K.

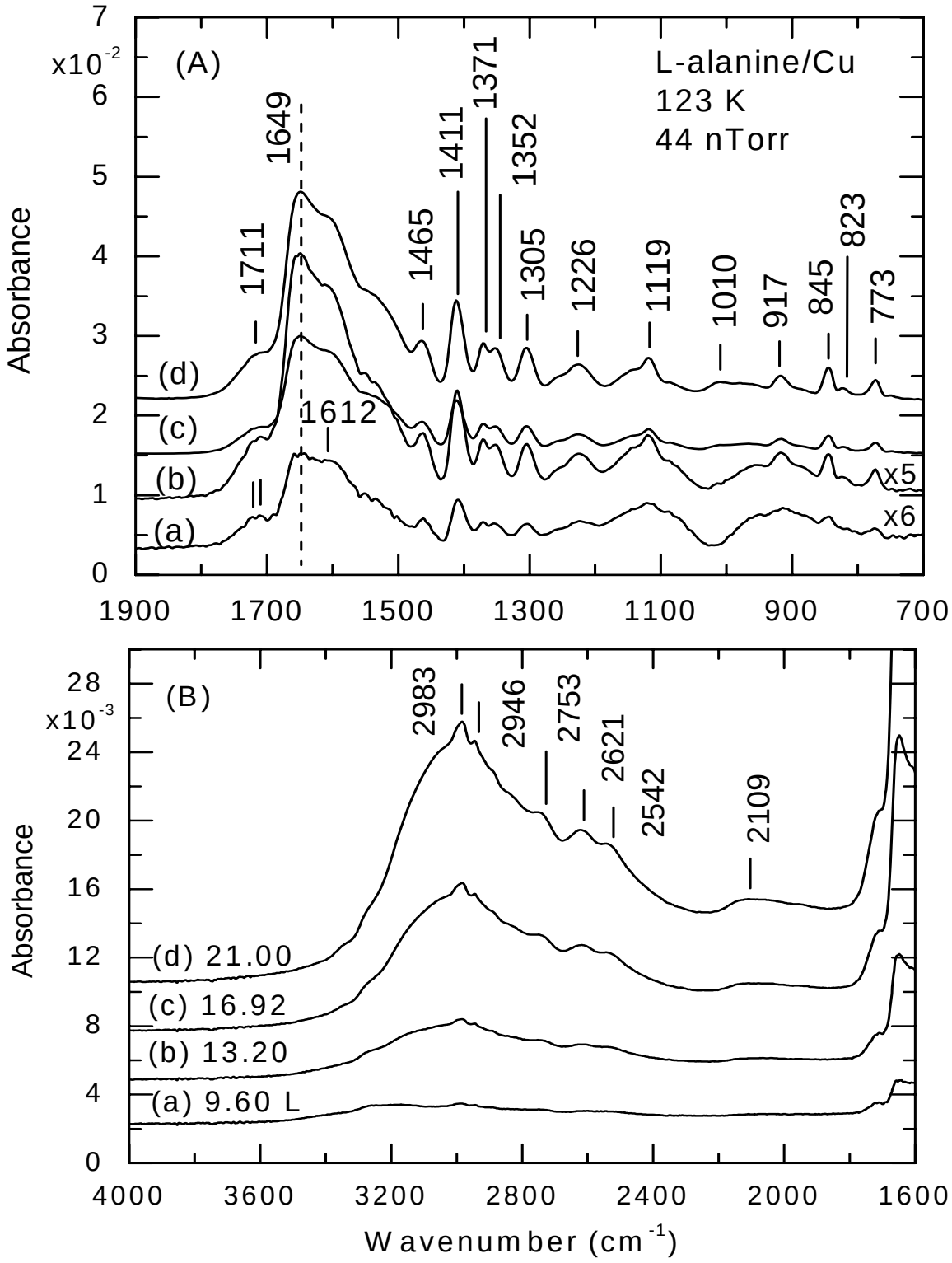

Figure 3.15: RAIRS spectra of (a) 9.60 L, (b) 13.20 L, (c) 16.92 L and (d) 21.00 L of L-alanine deposited on polycrystalline Cu at 123 K.

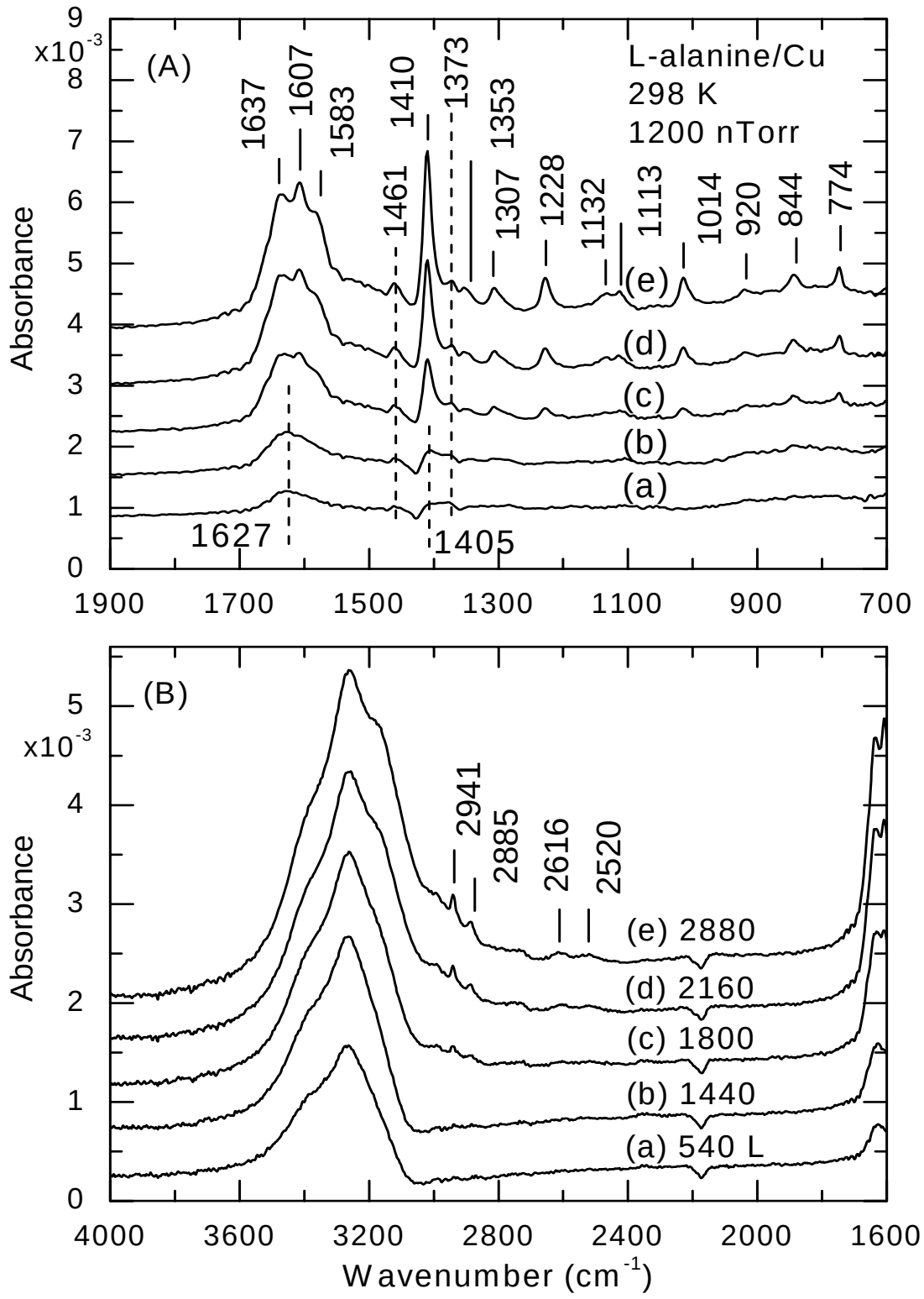

Figure 3.16: RAIRS spectra of (a) 540 L, (b) 1440 L, (c) 1800 L, (d) 2160 L and (e) 2880 L of L-alanine deposited on polycrystalline Cu at 298 K.

Table 3.2: Assignments of experimental vibrational features of L-alanine evaporated on polycrystalline Cu at 123 K and 298 K.

L-alanine/Cu at 123 K		L-alanine/Cu at 298 K	
Assignment [Refs 44, 49, 50, 51, 52, 53]	Vibrational modes (cm^{-1})	Assignment [Refs 44, 49, 50, 51, 52, 53]	Vibrational modes (cm^{-1})
ν_{as} (CH_3) / ν_s (NH_3^+)	2983	ν_s (CH_3)	2941
ν_{as} (CH_3)	2946	δ (CH_3)	2885
ν (CH)	2897	ν_{as} (COO^-)	1637
ν (C=O)	1712	ν_{as} (COO^-)	1607
δ (NH_2)	1649	δ (NH_2)	1583
δ_{as} (CH_3)	1465	δ_{as} (CH_3)	1461
δ (CH) + δ_{as} (CH_3)	1411	ν_s (COO^-) + δ_s (CH_3)	1410
δ_{as} (CH_3) + δ (CH)	1371	δ_s (CH_3) + ν_s (COO^-)	1373
δ (CH)	1352	δ (CH) + ν_s (COO^-)	1307
δ (CH)	1305	ν (C–O)	1228
γ (NH_2)	1226	ρ (NH_3^+)	1132
ν (CN)	1119	ρ (NH_3^+)/ ν (CC)	1113
ρ (CH_3)	1010	ρ (CH_3)/ν (CN)	1014
ν (C–CH_3)	917	ν (CN) + δ_s (COO^-) [+ ρ (CH_3)]	920
ω (NH_2)	845	δ_s (COO^-) + ν (CN)/ ν_{as} (CCN)	844
ν (C–COOH)	823	δ (COO^-) + ν (CC)	774
ω (COO)	773		

Key: ν_{as} = asymmetric stretching mode, ν_s = symmetric stretching mode, ν = stretching mode, δ = scissoring mode, ω = wagging mode, δ_s = symmetric deformation mode, δ_{as} = asymmetric scissoring mode, ρ = rocking mode, γ = twisting mode

3.8 Adsorption of L-alanine on non-crystalline ice

The vibrational spectra of L-alanine adsorption on a NCI surface are presented in Figure 3.17. As discussed earlier for the case of glycine, termination of an ice surface with foreign molecules results in the ice spectrum lacking the sharp feature at 3696 cm^{-1}, which comes from the stretching mode of the dangling OH bonds at the surface. This is clearly seen for the case of the adsorption of L-alanine on NCI as well, indicated by the inset in Figure 3.17 (B). Before exposure, the sharp peak at 3696 cm^{-1} is easily identified, but reduces in intensity as L-alanine are exposed to the ice film. Complete extinction of this particular feature is seen after 4.80 L exposure, which suggests that all the OH dangling bonds are occupied. A different behaviour is observed for the OH stretching band at 3393 cm^{-1}, which initially shows a small increase in intensity, but weakens gradually once the free OH bonds become saturated. This is understood as the adsorbed species being involved in stronger interaction with the ice film. Upon completion of saturating the OH dangling bond, further exposure to 4.80 L produces a new set of features in the 1800–1100 cm^{-1} region appear. This observation allows recognition of the fact that the adsorbed species is now interacting with the surface bilayer of the ice film. This is consistent with earlier observations made for the glycine species. This interpretation may also be confirmed by the decrease in intensity of the OH bending mode at 2234 cm^{-1} [Figure 3.17 (B) (e)]. As in the case of glycine, a neutral L-alanine adspecies is believed to bind to the NCI film, evidenced by the weak carbonyl stretching vibration of the COOH group at 1712 cm^{-1}. The appearance of the band appearing at 1652 cm^{-1}, assigned to NH_2 scissoring mode, and the carbonyl stretching mode at an early

stage of exposure is understood as an interaction between the functional groups and the ice film.

With further L-alanine exposure, the OH stretching band at 3393 cm^{-1} was found to decrease gradually (Figure 3.18). This is an indication that the ice film is melting partially, which was expected as the "warm" species land on the cold substrate. On the other hand, the vibrational bands in the 1900–700 cm^{-1} region become more distinct. At 22.3 L exposure, the emerging bands are found to be located at 1712, 1648, 1465, 1412, 1371, 1353, 1305, 1227, 1119, 846 and 774 cm^{-1}. These peaks have been previously seen for the adsorption of L-alanine at 123 K on the Cu support and the assignments given in Table 3.2. As larger amounts of L-alanine species bind to the NCI surface (at 31.9 L exposure), the OH stretching band is affected. We interpret the reduction of this peak intensity as a stronger interaction of the adsorbate with the substrate, which therefore leads to the appearance of new features, particularly in the fingerprint region. Moreover, the peaks at 2984 and 2946 cm^{-1} appear to grow in the high-wavenumber region at 31.9 L exposure. At 40.8 L exposure, a series of distinguishable IR bands are observed, which is accompanied by the hump at 2234 cm^{-1} being quenched. The latter is assigned to the combination band of the ice film. This confirms the fact that the adsorbate is highly involved in binding to the ice film. Consequently, a new hump grows at 2136 cm^{-1}, which increases in intensity with further exposure. At 57.0 L exposure, the intensity of the L-alanine related peaks continue to increase in intensity, which can be attributed to multilayer formation since the shape of the RAIRS spectra are similar for higher exposure phase.. In addition, the band at 2136 cm^{-1} becomes evident, and may be attributed to hydrogen bonding interaction between adjacent L-alanine species within the

multilayer. However, if we compare the intensities of the features at 2234 and 2136 cm^{-1}, the higher intensity of the band at 2234 cm^{-1} indicates that the former band is stronger than the latter one. We hypothesize that the interaction between the water molecules in the NCI film is stronger than the corresponding molecular interaction in the L-alanine overlayer. The IR absorption bands related to the L-alanine adsorption on NCI are very similar to those obtained for that on polycrystalline Cu at low temperature.

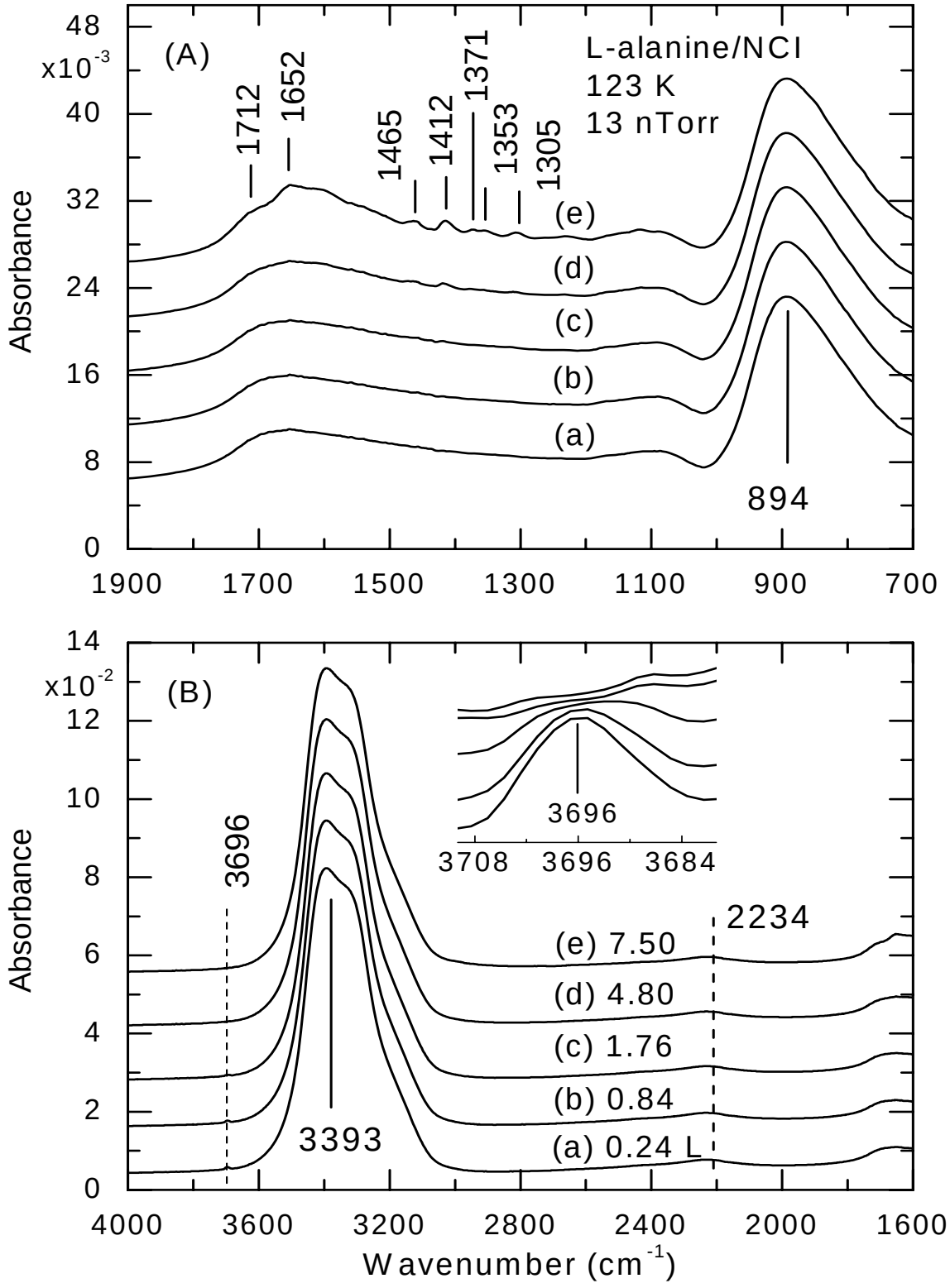

Figure 3.17: RAIRS spectra of (a) 0.24 L, (b) 0.84 L, (c) 1.76 L, (d) 4.80 L and (e) 7.50 L of L-alanine deposited on NCI at 123 K.

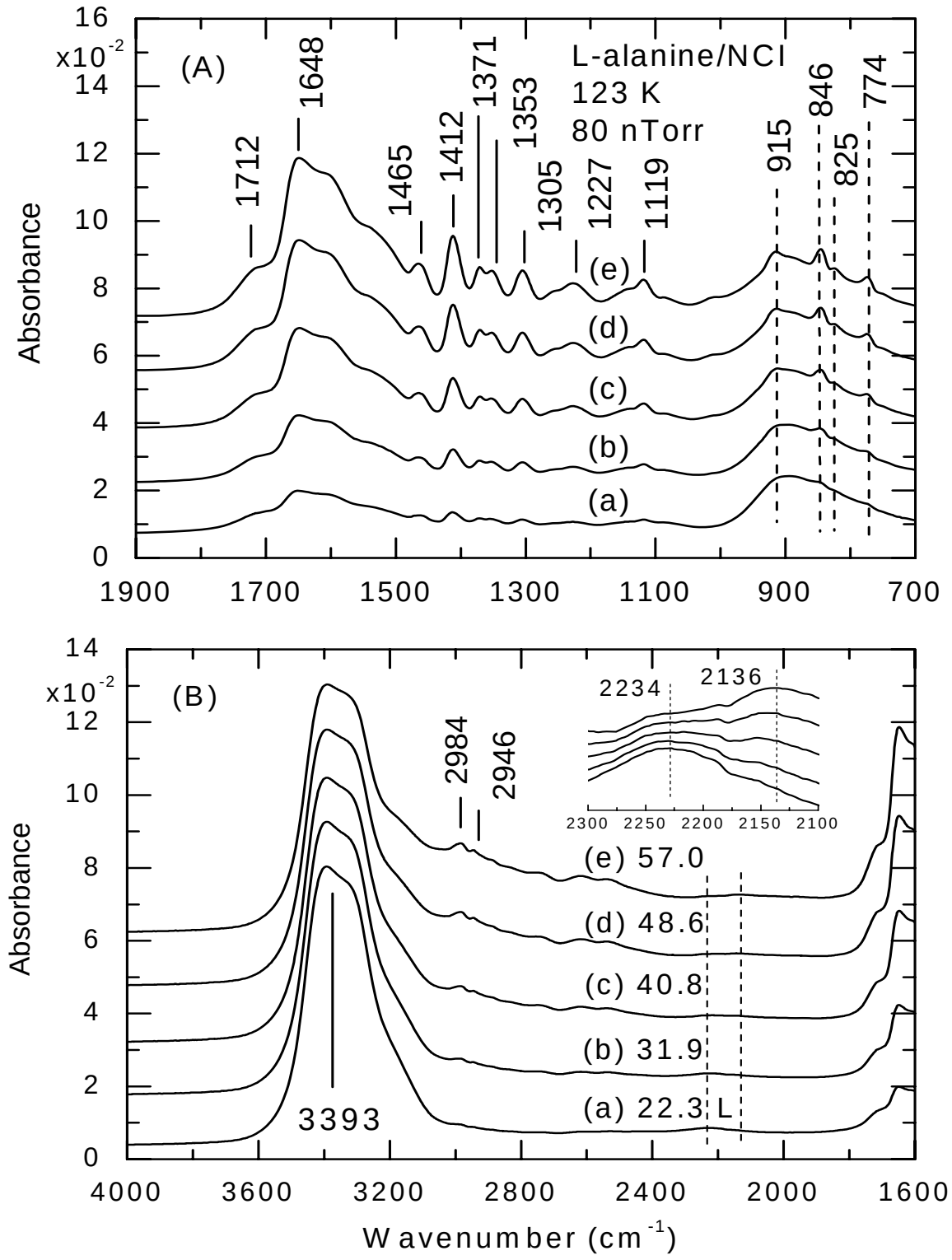

Figure 3.18: RAIRS spectra of (a) 22.3 L, (b) 31.9 L, (c) 40.8 L, (d) 48.6 L and (e) 57.0 L of L-alanine deposited on NCI at 123 K.

3.9 Thermal evolution of L-alanine on non-crystalline ice

Annealing L-alanine deposited on a NCI film at 118 K gives rise to irreversible changes in the infrared spectra, starting at 130 K and completing at above 326 K. As one can imagine, termination of an ice surface with L-alanine species results in the ice spectrum lacking the dangling OH bonds and thus no IR peaks are seen in this region. The bottom spectrum represents the spectrum obtained after deposition of L-alanine at 118 K. When the sample is annealed to 130 K, no significant changes are observed in the band shape for the RAIRS spectra in the low-wavenumber region [Figure 3.19 (A) (b)], but the intensities of the OH stretching band and some related L-alanine related peaks in the high-wavenumber region [Figure 3.19 (B) (b)] do change with temperature. However, upon annealing to 164 K, the shape of the OH stretching band is different from the one at 130 K. The latter peak at 3390 cm^{-1} lowers in intensity until the absorption band reaches a plateau in its intensity which is maintained in the 3400–3320 cm^{-1} region upon heating to 164 K. This observation can be described as the onset of crystallization. The latter description is also evidenced by the sudden growth of the shoulder at 2107 cm^{-1}. The spectrum shown as Figure 3.19 (B) (e) can be interpreted as complete transformation of the ice film upon annealing to 172 K, which is confirmed by the growth of the OH stretching band of PCI at 3284 cm^{-1}. However, it should be noted that the peak is not as strong as for a freshly prepared PCI film on a metal surface because of the L-alanine species embedded on the surface bilayer of the ice film. Figure 3.19 (A) (c) demonstrates the effect of annealing the sample to 164 K in the low-wavenumber region. The evolution of the spectrum from 118 K to 172 K shows that the transformation of the NCI film is accompanied by an increase in the intensity of the NH_2 scissoring band at 1652 cm^{-1}. The

spectrum is also characterized by a discernible peak at 1542 cm^{-1}, attributed to NH_3^+ scissoring mode, which was seen earlier as a shoulder during the adsorption process. In addition the features at 1257 and 1087 cm^{-1} are found to diminish upon annealing. Most importantly is the decrease in the C=O stretching band at 1712 cm^{-1} band, which can be explained as the loss of the proton from the –COOH acid group.

A series of RAIRS spectra produced at higher annealing temperature are illustrated in Figure 3.20. When annealed at 182 K, the band at 3284 cm^{-1} disappears while a shoulder still exists at 3380 cm^{-1}, which may be interpreted as partial desorption of the ice film. The latter change is accompanied by a small increase in intensity of the L-alanine related peaks in the high-wavenumber region. This partial desorption behavior of the ice film can be confirmed by closely analyzing the low-wavenumber region. While the band shape in the low-wavenumber region remains unchanged, the hump at 894 cm^{-1} for the ice film [Figure 3.17 (A)] which was masked by the growth of L-alanine peaks in the fingerprint region, appears to decrease in intensity. The latter band was assigned to the librational mode for a bare ice film. Moreover, at 182 K, the proton transfer process is still taking place, evidenced by the continued presence of the band at 1712 cm^{-1} but in reduced intensity. After annealing to 291 K, the hump at ~ 3380 cm^{-1} weakens considerably, which suggests that the ice film is evacuated from the surface. A decrease in intensity is also observed for the peaks associated with the L-alanine species in the high-wavenumber region. Along with the decrease in intensity, the bands at 2107 cm^{-1} is red-shifted to 2086 cm^{-1}, respectively upon annealing to 182 K. In conjunction with these changes, a few modifications are also observed for the L-alanine peaks in the low-wavenumber region. Firstly, the disappearance of the shoulder at 1712 cm^{-1} may be

envisaged as the completion of the proton transfer. Secondly, the absence of the shoulder at 1610 cm^{-1} suggests that a different orientation of the adspecies on the surface upon desorption of the ice film. Further justification for this interpretation is the peak at 1542 cm^{-1} which undergoes a red-shift by 7 cm^{-1} and sharpens upon annealing to 291 K. The most interesting aspect is the band at 1652 cm^{-1}, which becomes more intense, again suggesting a different orientation of the adsorbed species. On further annealing to 309 K [Figure 3.20 (c)], the bands related to L-alanine start to decay, which implies that the material is leaving the surface. This is further elaborated by the spectrum resulting from a 326 K anneal [Figure 3.20 (d)], where a general reduction in intensity is observed for all the peaks, confirming the desorption of L-alanine adspecies from the metal surface. On the basis of the above discussion, we may suggest a similar explanation for the thermal induced spectral evolution found for the L-alanine adspecies as that for glycine adspecies on ice. The ice film becomes liquid-like as it is heated, making it feasible for the L-alanine adspecies to undergo solvation such that the neutral form of the molecule is transformed to the zwitterionic form during annealing.

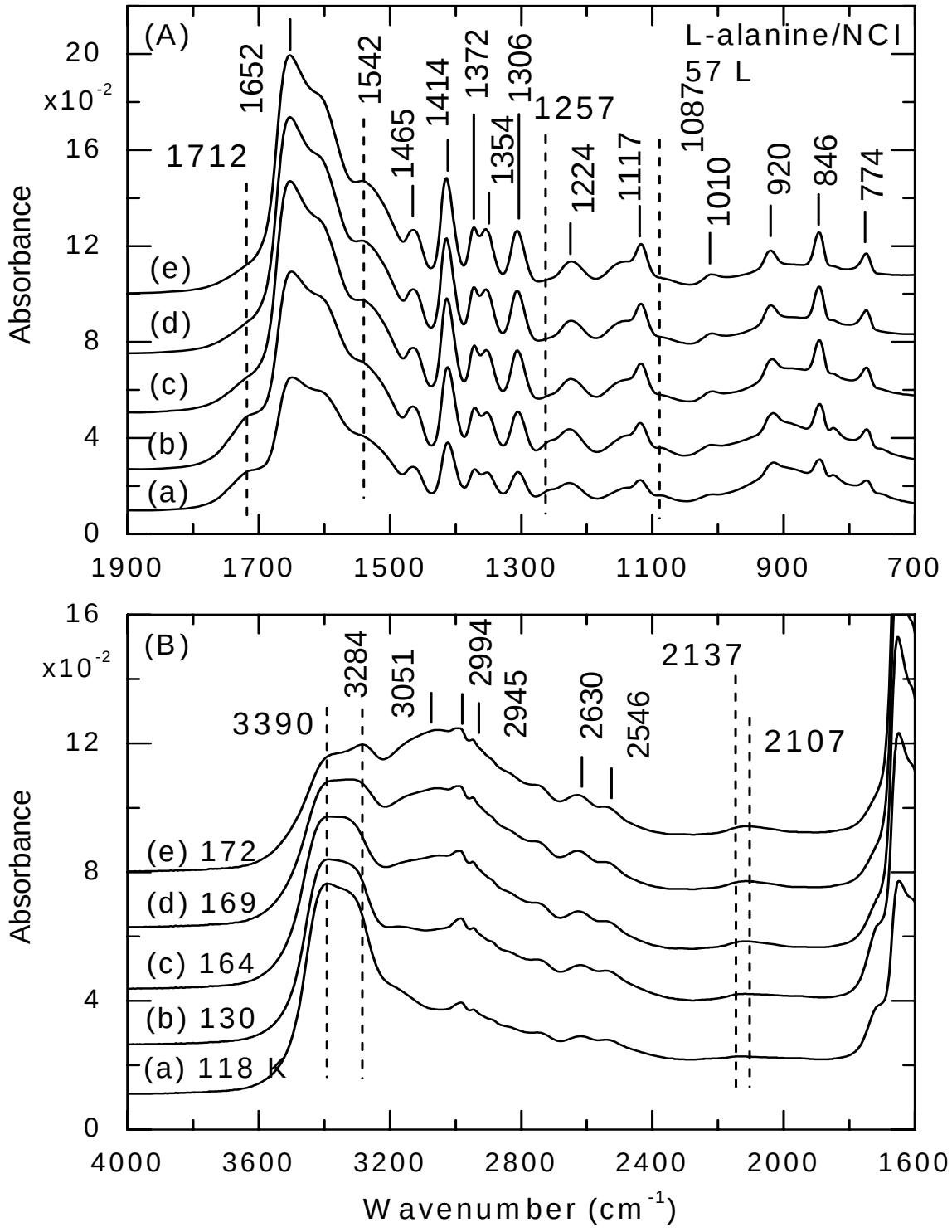

Figure 3.19: RAIRS spectra of L-alanine deposited at 13 nTorr on a NCI film at 123 K as a function of annealing temperature: (a) 118 K, (b) 130 K, (c) 164 K, (d) 169 K and (e) 172 K.

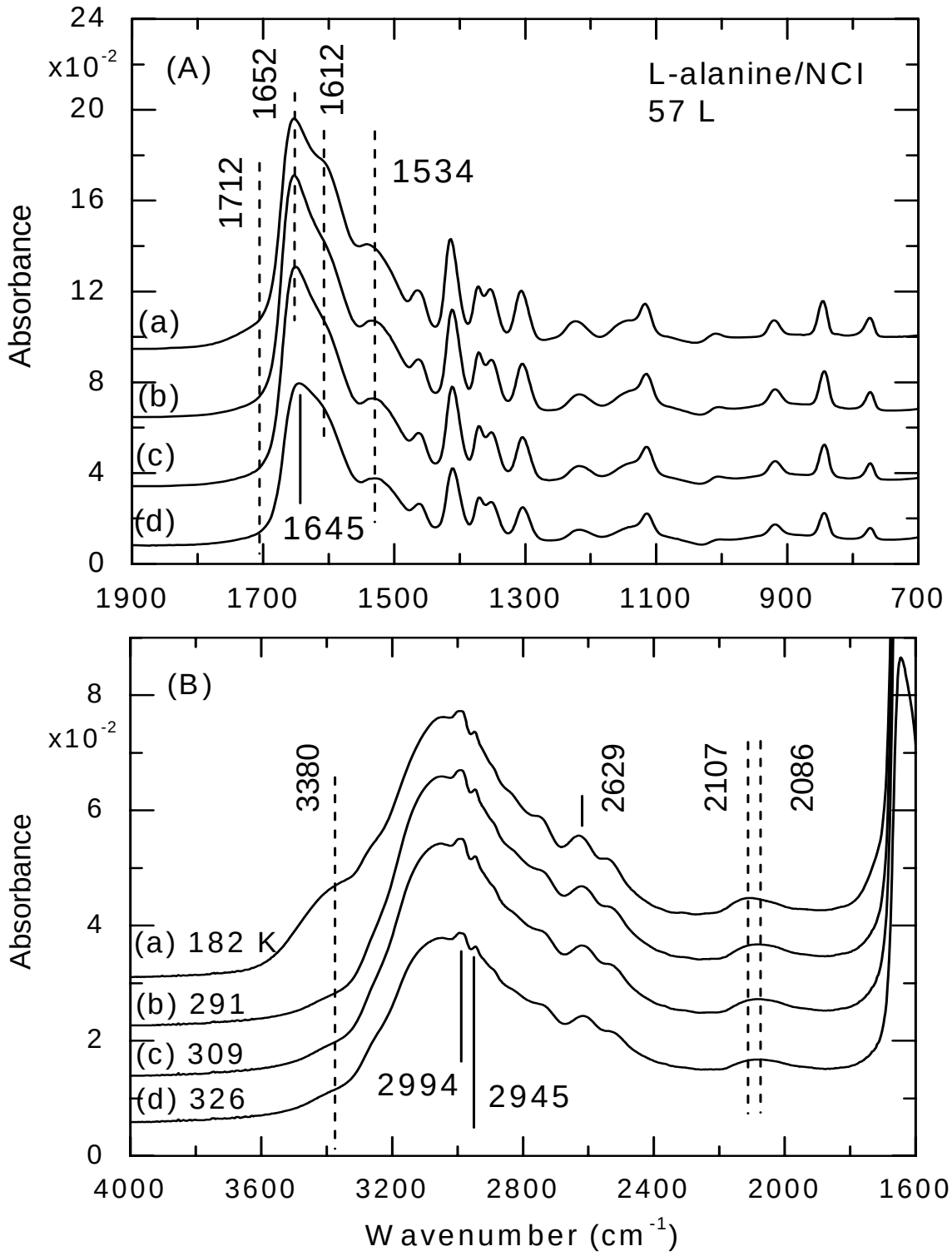

Figure 3.20: RAIRS spectra of L-alanine deposited at 13 nTorr on a NCI film at 123 K as a function of annealing temperature: (a) 182 K, (b) 291 K, (c) 309 K and (d) 326 K.

3.10 Adsorption of L-alanine on polycrystalline ice

Studies of L-alanine adsorption on PCI films at 155 K by RAIRS has led to similar conclusions to that carried out for glycine adsorption on PCI film. It has been shown that the signal from the free OH group at 3693 cm^{-1}, which is sensitive to foreign molecules, decreases initially for the 7.68 and 13.50 L exposure and is finally suppressed upon adsorption of L-alanine species after 13.50 L exposure [Figure 3.21 (B)]. This decrease is consistent with the fact that the free OH would give rise to hydrogen bonding interaction between the ice surface and the adsorbed species. The peaks at 1720 and 1650 cm^{-1} are among the first few bands that appear at an early stage. They are attributed to the C=O stretching and NH_2 scissoring modes, respectively, of the compound under investigation and therefore we would suggest that both NH_2 and COOH functional groups interact with the OH dangling bond of the ice surface via hydrogen bonding. The infrared spectra also reveal that the number of interacting L-alanine molecules does have an effect on the ice structure. This is clearly indicated by the combination band at 2231 cm^{-1} and libration mode at 884 cm^{-1}, which become reduced in intensities as a result of interaction between the substrate and the adsorbate. In addition to these observations, other notable differences in infrared absorption bands become evident with further L-alanine exposure. In particular, Figure 3.21 (B) shows changes in the peak position and the intensity of the OH stretching band, such that a red-shift of 5 cm^{-1} is observed from 13.50 to 24.48 L exposure. This is correlated with the appearance of several peaks in the fingerprint region, attributed to the L-alanine species. This can be interpreted as the formation of extensive hydrogen bonding interactions of the surface bilayer and the adsorbate. The disappearance of the OH dangling mode confirms the fact that the surface is fully

terminated with L-alanine species, and therefore the other incoming adorbate will interact with the surface bilayer. The decrease in the combination band at 2231 cm^{-1} for the ice film and the appearance of a hump at 2112 cm^{-1} for the 31.08 L exposure also account for the hydrogen bonding interaction between the L-alanine species. It should be noted that all the L-alanine related features become distinct at 24.48 L exposure. The RAIRS spectrum for the 31.08 L exposure resembles that for the 24.48 L exposure with increased intensity of the bands, continuing multilayer formation as the shape of the RAIRS spectra for the high exposure phases are similar.

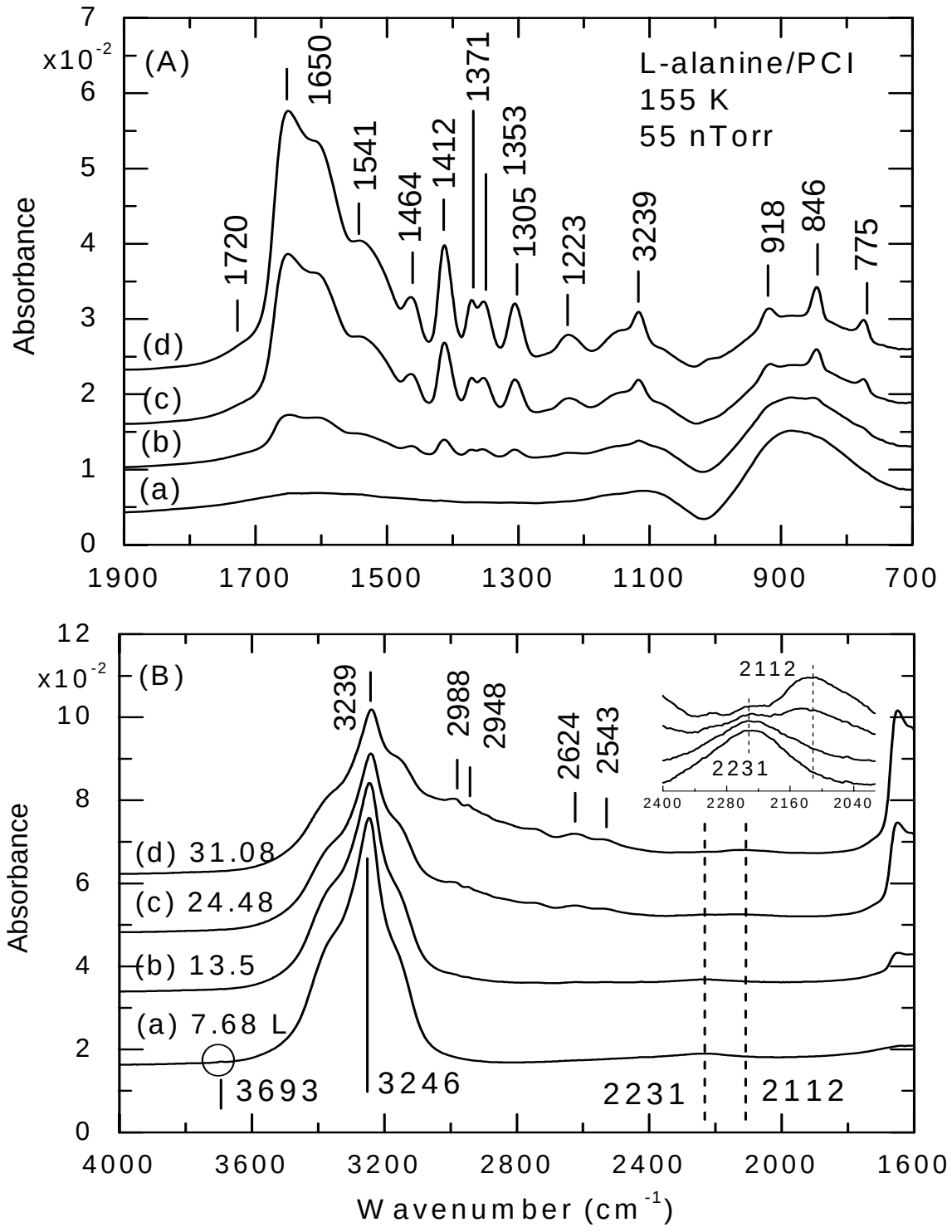

Figure 3.21: RAIRS spectra of (a) 7.68 L, (b) 13.50 L, (c) 24.48 L and (d) 31.08 L of L-alanine deposited on PCI at 155 K.

3.11 Thermal evolution of L-alanine on polycrystalline ice

In Figure 3.22, the spectrum of L-alanine deposited on PCI at 128 K is compared with the spectra of the sample after annealing to different temperatures, namely at 156, 170, 298, 310 and 316 K. It can be observed that the shape of the IR absorption bands for the annealed samples at 156 K [Figure 3.22 (b)] is quite similar to the as-deposited sample at 128 K, with only a few peaks showing small changes in the low-wavenumber region. In particular, a small decrease in intensity of the C=O stretching band at 1720 cm^{-1} is observed. The OH stretching band also undergoes a decrease in intensity at 156 K. Moreover, the NH_2 scissoring band at 1649 cm^{-1} band shows a small increase in intensity. The remaining features appear unaffected upon annealing to 156 K, indicating that only the ice film and the proton-transfer process are sensitive at that temperature. Upon further annealing to 170 K, the NH_2 scissoring mode at 1649 cm^{-1} continues to grow and the weak COO^- asymmetric stretching mode at 1613 cm^{-1} becomes more distinct. No bands associated with the OH stretching vibration of the ice film can be observed at that stage which indicates complete desorption of the ice film from the surface. We also notice a hump appearing at 3041 cm^{-1}, which was previously attributed to intermolecular interaction within the multilayer in the case of glycine at 170 K. The sample annealed to 296 K is marked by a number of changes occurring in the RAIRS spectrum [Figure 3.22 (d)]. Firstly, the reduction in intensity of the bands in the 4000–2000 cm^{-1} region, accompanied by a red-shift of the 2115 cm^{-1} band to 2084 cm^{-1} indicates that the L-alanine species are undergoing re-orientation on the surface after complete desorption of the ice film. Moreover, the band at 1530 cm^{-1} increases in intensity. It is interesting to note the disappearance of the 1613 cm^{-1} feature, assigned to the COO^- asymmetric

stretching mode, at 296 K. On the other hand, the NH_2 scissoring band at 1649 cm^{-1} continues to increase in intensity. This continued growth is in accordance with the proton-transfer phenomenon, whereby the proton from the carboxylic group is transferred to the amino group. On the other hand, it appears that some bands in the 1500-700 cm^{-1} region are unaffected by higher annealing temperature, while others undergo small red-shifts. However, it should be noted that no drastic changes are observed at 296 K, which is effectively room temperature, as was observed for glycine. It should also be noted that at that particular annealing temperature, the C=O stretching mode has completely disappeared, which suggested that the proton transfer has taken place. Upon annealing to 316 K [Figure 3.22 (f)], no significant changes can be seen, with the exception that the L-alanine related peaks are seen to lower in intensity. This is attributed to desorption of L-alanine from the Cu surface.

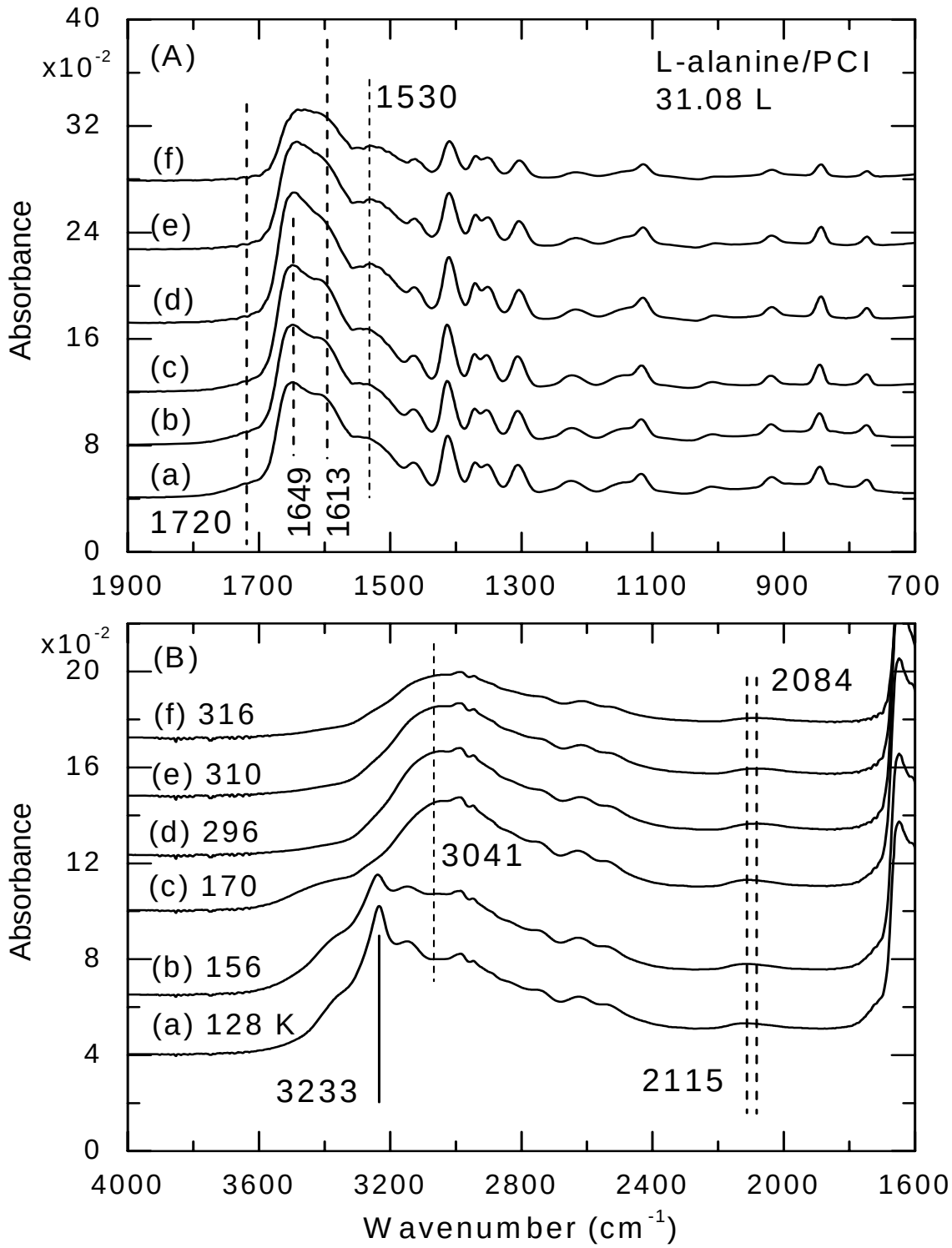

Figure 3.22: RAIRS spectra of 31.08 L of L-alanine deposited at 55 nTorr on a PCI film at 155 K as a function of annealing temperature: (a) 128 K, (b) 156 K, (c) 170 K, (d) 296 K (e) 310 K and (f) 316 K.

3.12 Comparison between the adsorption of L- and D-alanine on NCI and PCI films

In addition to L-alanine adsorption on the NCI and PCI surfaces described above, we have also collected RAIRS spectra for D-alanine subjected to the same type of treatments. It should be noted that both L- and D-alanine behave in a similar fashion on NCI and PCI films, as shown by the Figures 3.23 and 3.24. This observation confirms the fact that adsorption of a chiral species on a non-chiral surface (ice surface in this case) does not affect the chirality. However, it would be better to compare the RAIRS spectra for similar exposure for the L- and D-alanine.

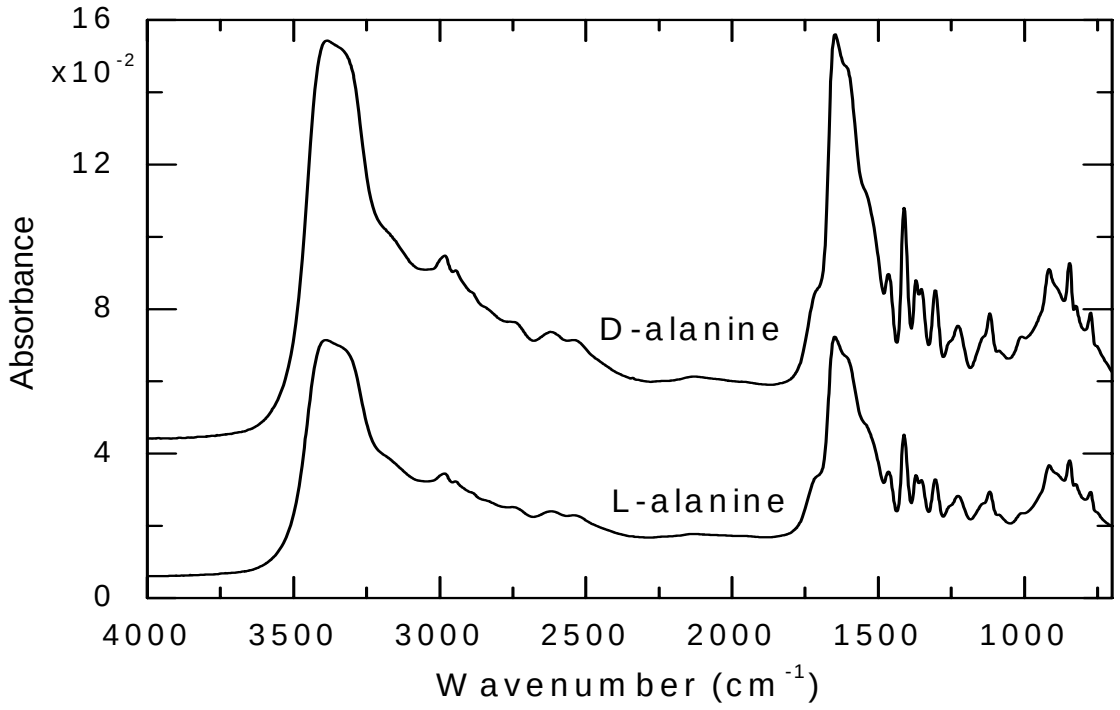

Figure 3.23: RAIRS spectra of 57.0 L of L-alanine and 15.96 L of D-alanine deposited on NCI at 120 K.

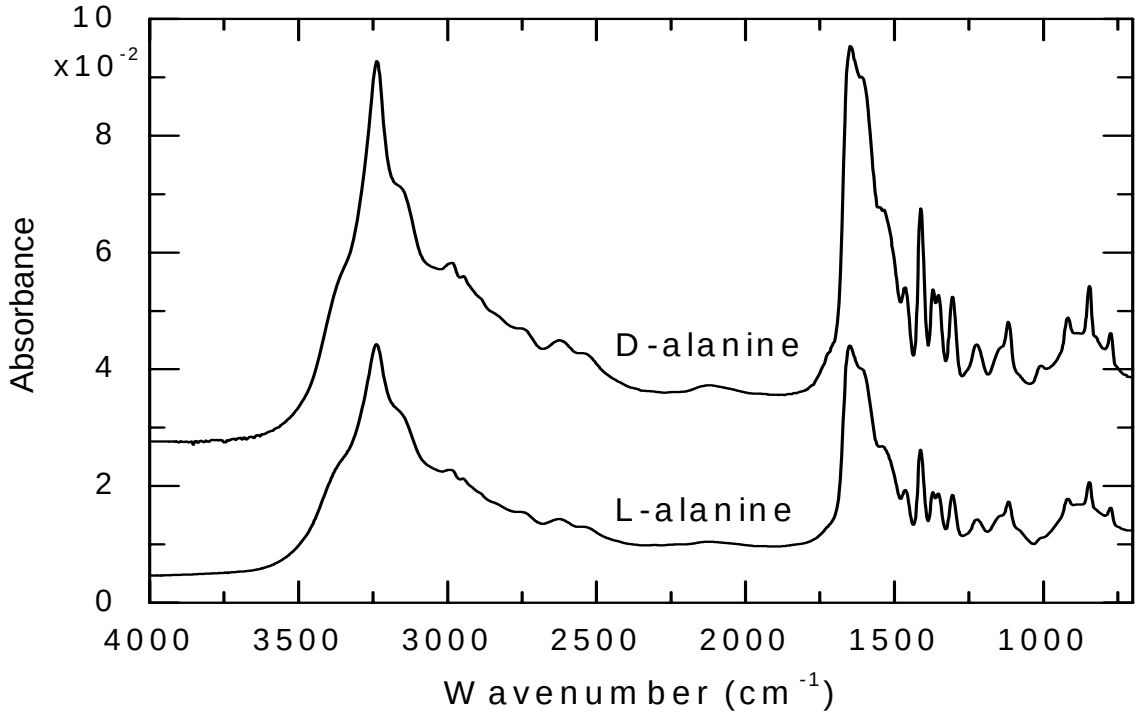

Figure 3.24: RAIRS spectra of 31.08 L of L-alanine and 35.1 L of D-alanine deposited on PCI at 155 K.

Chapter 4

Conclusion and Future work

The goal of the present work was to carry out a comprehensive investigation of the surface chemistry of two of the most fundamental amino acids on ice surfaces using the technique of Reflection-Absorption Infrared Spectroscopy. It is well recognized that infrared spectroscopy is a powerful tool for studying the adsorption of a reactant on a surface [54]. The present experiments were carried out under UHV conditions, and the ice film was deposited onto a polycrystalline Cu disk under these conditions. All three molecules studied, namely glycine, L-alanine and D-alanine, are found to bind to the ice surface via hydrogen bonding. The disappearance of the dangling OH of ice at 3696 cm^{-1} and the appearance of the C=O stretching vibration in the 1710–1723 cm^{-1} region suggests that the carboxylic group is initially involved in bonding to the surface. The presence of the carbonyl peak also indicates that the amino acid species are adsorbed in the neutral form on the ice surface. The strong interaction of the amino group of the adspecies with the ice film is also thought to occur, which is evidenced by the appearance of the NH_2 scissoring infrared band at 1660 cm^{-1}. Evidently, with further exposure, these strongly hydrogen-bonded adsorbates readily interact with the surface bilayer of the ice film, leading to reconstruction of the ice structure. The continuous growth of the IR peaks of the adspecies is recognized as multilayer formation evidenced by the band appearing near 3000 cm^{-1}.

The next sets of experiments addressed thermally induced desorption of amino acid from the ice surface. These experiments revealed an important aspect of the system multilayer, the proton transfer at the carboxylic site of the amino acids. Proton transfers

are important in chemistry and biology because they are involved in almost every biological mechanism [55, 56]. The infrared spectral changes described in the present work lead us to the conclusion that the following thermally induced reaction is occurring at ~300 K. It was shown that the proton transfer was significantly assisted by the ice film which becomes liquid-like as heat is introduced to the substrate, to allow the process to occur at room temperature.

In addition to the adsorbates-on-ice experiments, the other set of experiments examine the effect of temperature of the Cu metal support on the amino acid film itself under UHV conditions. The room temperature data indicated an ionic adspecies on the polycrystalline Cu surface, which was evidence by the absence of the C=O stretching mode, suggesting deprotonation of the carboxylic group occurring at 300 K, leading to the COO^- species. However, it was difficult to distinguish between the NH_2 and NH_3^+ groups as they appear in the same wavenumber region. Moreover, the molecular arrangement of the adsorbed species was found to be dependent on the coverage. In contrast, low-temperature experiments produced a neutral adsorbed species, which was similar to that found in the ice experiments.

Following the RAIRS measurements, it would be interesting to correlate the infrared observations with the future TPD experiments (by means of mass spectrometry) in order to provide better insights into the processes taking place as the substrate is warmed up. Moreover, we can also try to better understand the adsorption and desorption processes by performing the experiments as a function of ice film thickness. The present work involves the study of the adsorption of amino acids on an ice film. It would be interesting to extend this work to a number of other studies involving an ice film

adsorbed on a layer of amino acid, and an ice film sandwiched between two amino acid films, and the effect of a sulphur-containing amino acid (cysteine) on the ice surface. Another interesting work involves the simultaneous adsorption of multiple amino acids on the ice film. However, this will require some modification to the present system because currently the UHV chamber consists of only one effusive cell, which can contain only one amino acid at a time. With such experiment, we might be able to follow whether there is peptide bond formation between these amino acids. In addition, it will be of great interest to study the adsorption of DNA base pairs (Adenine-Thymine and Guanine-Cytosine) on ice film. Again, this would require changes to the present system, since the DNA base pairs having higher melting point than simple amino acids will cause the ice film to desorb from the Cu support, before any adsorption process could take place.

References

[1] D. G. Castner, B. D. Ratner, Surf. Sci. 500 (2002) 28.

[2] B. Kasemo, Surf. Sci. 500 (202) 656.

[3] Y. J. Kuan, S. B. Charnley. H. C. Huang, L. Tseng, Z. Kisiel, Astrophy. J. 593 (2003) 848.

[4] L. E. Snyder, F. J. Lovas, J. M. Hollis, Astrophys. J. 619 (2005) 914.

[5] G. Tzvetkov, M. G. Ramsey, F. P. Netzer, Chem. Phys. Lett. 397 (2004) 392

[6] X. Wei, Y. R. Shen, Appl. Phys. B 74 (2002) 617.

[7] Y. Marechal, The Hydrogen Bond and the Water Molecule, The Physics and Chemistry of Water, Aqueous and Bio Media, Elsevier, 1st Edition, 2007.

[8] T. Loerting, N. Giovambattista, J. Phys.: Condens. Matter 18 (2006) R919.

[9] L. Schriver-Mazzuoli, A. Schriver, A. Hallou, J. Mol. Struct. 554 (2000) 289.

[10] J. P. Devlin, J. Geophys. Res. 106 (2001) 33333.

[11] S. Mitlin, K. T. Leung, J. Phys. Chem. B 106 (2002) 6234.

[12] B. Mate, A. Medialdea, M. A. Moreno, R. Escribano, V. J. Herrero, J. Phys. Chem. B 107 (2003) 11098.

[13] S. Mitlin, K. T. Leung, Can. J. Chem. 82 (2004) 978.

[14] N. Horimoto, H. S. Kato, M. Kawai, J. Chem. Phys. 116 (2002) 4375.

[15] G. Bode, G. Ann. Phys. 30 (1909) 326.

[16] C. A. Angell, Annu. Rev. Phys. Chem. 55 (2004) 559.

[17] M. M. Thiam, T. Kondo, N. Horimoto, H. S. Kato, M. Kawai, J. Phys. Chem. B 109 (2005) 16024.

[18] L. Delzeit, K. Powell, N. Uras, J. P. Devlin, J. Phys. Chem. B 101 (1997) 2327.

[19] N. Uras, V. Buch, J. P. Devlin, J. Phys. Chem. B 104 (2000) 9203.

[20] S. Mitlin, K. T. Leung, J. Phys. Chem. B 106 (2002) 6234.

[21] C. Martin, C. Manca, P. Roubin, Surf. Sci. 502-503 (2002) 275.

[22] C. Martin, C. Manca, P. Roubin, Surf. Sci. 502-503 (2002) 280.

[23] J. Cyriac, T. Pradeep, J. Phys. Chem. C (2007) A.

[24] L. Delzeit, M. S. Devlin, B. Rowland, J. P. Devlin, J. Phys. Chem. 100 (1996) 10076.

[25] H. Ogasawara, N. Horimoto, M. Kawai, J. Chem. Phys. 112 (2000) 8229.

[26] A. Coupeaud, N. Pietri, A. Allouche, J. P. Aycard, I. Couturier-Tamburelli, J. Phys. Chem. A 112 (2008) 8024.

[27] T. J. Millar, J. M. C. Rawlings, A. Bennett, P. D. Brown, S. B. Charnley, Astron. Astrophys., Suppl. Ser. 87 (1991) 585.

[28] S. Mitlin, K. T. Leung, Surf. Sci. 505 (2002) L227.

[29] Q. Gao, K. T. Leung, J. Phys. Chem. B 109 (2005) 13263.

[30] G. Tzvetkov, M. G. Ramsey, F. P. Netzer, J. Chem. Phys. 122 (2005) 114712.

[31] J. P. Devlin, V. Buch, J. Phys. Chem. B 101 (1997) 6095.

[32] B. A. Garetz, J. Matiac, Phys. Rev. Lett. 89 (2002) 175501-1.

[33] V. Efstathiou, D. P. Woodruff, Surf. Sci. 531 (2003) 304.

[34] K. S. Kumar, T. Raghavalu, V. Mathivanan, M. Kovendhan, B. Sivakumar, G. R. Kumar, S. G. Raj, R. Mohan, J. Crys. Gro. 310 (2008) 1182.

[35] J.-H. Kang, R. L. Toomes, M. Polcik, M. Kittel, J.-T Hoeft, V. Efstathiou, D. P. Woodruff, A. M. Bradshaw, J. Chem. Phys. 118 (2003) 6059.

[36] S. M. Barlow, K. J. Kitching, S. Haq, N. V. Richardson, Surf. Sci. 401 (1998) 322.

[37] J. D. Meyer, S. J. Bai, M. Rani, R. Suryanarayanan, R. Nayar, J. F. Carpenter, M. C. Manning, J. Pharma. Sci. 93 (2004) 1359.

[38] P. Ehrenfreund, M. P. Bernstein, J. P. Dworkin, S. A. Sanford, L. J. Allamandola, Astro. J. 550 (2001) L95.

[39] K. Uvdal, P. Bodo, A. Ihs, B. Liedberg, W. R. Salaneck, J. Colloid Interface Sci. 140 (1990) 207.

[40] G. Jones, S. J. Jenkins, D. A. King, Surf. Sci. Lett. 600 (2006) L224.

[41] A. His, B. Liedberg, K. Uvdal, C. Törnkvist, P. Bodö, I. Lundström, J. Colloid Interface Sci. 140 (1990) 192.

[42] P. Löfgren, A. Krozer, J. Lausmaa, B. Kasemo, Surf. Sci. 370 (1997) 277.

[43] A. Gómez-Zavaglia, R. Fausto, Phys. Chem. Chem. Phys. 5 (2003) 3154.

[44] J. Williams, S. Haq, R. Raval, Surf. Sci. 368 (1996) 303.

[45] H. Iwai, M. Tobisawa, A. Emori, C. Egawa, Surf. Sci. 574 (2005) 214.

[46] P. V. Hobbs, Ice Physics, Clarendon, Oxford, 1974.

[47] J. E. Schaff, J. T. Roberts, J. Phys. Chem. 98 (1994) 6900.

[48] C. Carlsson, B. Liedberg, Mikrochim. Acta I (1988) 149.

[49] S. M. Barlow, S. Louafi, D. Le Roux, J. Williams, C. Muryn, S. Haq, R. Raval, Suf. Sci. 590 (2005) 243.

[50] S. Kumar, A. K. Rai, S. B. Rai, D. K. Rai, A. N. Singh, V. B. Singh, J. Mol. Struct. 791 (2006) 23.

[51] X. Cao, G. Fischer, Spectrochimica Acta A 55 (1999) 2329.

[52] M. T. S. Rosado, M. L. R. S. Duarte, R. Fausto, J. Mol. Struct. 410-411 (1997) 343.

[53] A. R. Garcia, R. Brito de Barros, J. P. Lourenço, L. M. Ilharco, J. Phys. Chem. A 112 (2008) 8280.

[54] E. M. McCash, Surface Chemistry, Oxford, 2001.

[55] P. M. Kiefer, J. T. Hynes, J. Phys. Chem. A 108 (2004) 11793.

[56] O. Y. Kwon, S. Y. Kim, K. T. No, Bull. Korean, Chem. Soc. 16 (1995) 410.